# Experiments and modeling of octanoic acid pyrolysis in a plug flow reactor

Julien Gornay, Pierre-Alexandre Glaude, Francis Billaud, Lucie Coniglio

# Experiments and modeling of octanoic acid pyrolysis in a plug flow reactor

*Julien Gornay, Pierre-Alexandre Glaude, Francis Billaud, and Lucie Coniglio**

Université de Lorraine - Ecole Nationale Supérieure des Industries Chimiques de Nancy, Laboratoire Réactions et Génie des Procédés UMR CNRS 7274, 1, rue Grandville BP 20451, 54001 Nancy Cedex, France

* To whom correspondence should be addressed. E-mail: lucie.coniglio@univ-lorraine.fr.

**Abstract**

Pyrolysis of carboxylic acids plays a key role in various industrial applications (production of bio-energy vectors from waste cooking oil reforming or of biosourced chemicals from lignocellulosic biomass pyrolysis, or even combustion of ethyl biodiesel). In this work, pyrolysis of octanoic acid selected as departure model compound was carried out in a plug flow reactor. Profiles of the reactant, stable intermediates, and final products, identified by gas chromatography/mass spectrometry, were measured by non-dispersive infrared absorption and gas chromatography equipped with thermal conductivity detector or flame ionization detector. Within the operating conditions of the plug flow reactor (mean pressure/kPa: 112; oven set point temperature/K: 923-1073, mean residence times/s: 0.42-0.83; reactant mole fraction in nitrogen selected as inert diluent: 3 and 5%), the major products formed are 1-olefins and carboxylic acids (saturated and monounsaturated) together with small species like hydrogen, carbon monoxide, carbon dioxide, methane, and ethylene. These experimental data were used to further develop a detailed chemical kinetic mechanism for octanoic acid pyrolysis, mainly

generated from EXGAS software with kinetic and thermodynamic properties of key reactions specific to carboxylic acids revisited. Satisfactory repeatability and material balances were obtained for the generated kinetic data, which also showed a satisfactory agreement with the proposed mechanism. Rate of production and sensitivity analyses were carried out for selected experimental conditions (high temperature and various residence times), highlighting the significant contribution of H-abstractions (particularly the α-hydrogens) and the sensitive key role of the unimolecular decomposition in octanoic acid consumption.

**Keywords:** pyrolysis; octanoic acid; chemical kinetics; experiments; plug flow reactor; modeling

## 1. Introduction

Mastering the thermal conversion of carboxylic acids is essential for various industrial applications, such as: *(i)* combustion of ethyl biodiesel for which carboxylic acids are intermediates formed during oxidation mechanism **[1-4]**; *(ii)* steam reforming and steam cracking of high free fatty acid waste cooking oil that were showed as totally green alternatives for the production of bio-energy vectors (gaseous fuel, hydrogen, or synthesis gas) **[5-6]**; *(iii)* pyrolysis of cellulosic and lignocellulosic biomass producing bio-oil which because of its high contents in carboxylic acids (up to 25 wt% **[7-8]**) needs first to be processed by deoxygenation to be used as transportation fuel **[9]**. While thermocatalytic- or hydrothermal-deoxygenation of carboxylic acids are well documented in the literature **[9-11]**, thermal deoxygenation (without catalyst) has received limited attention **[12]**.

Nevertheless, simulation, design, and analysis of processes involving chemical reactions need accurate information on the reactor unit but also on the thermophysical and kinetic properties of the reactive system under concern. Generation of experimental information is expensive, time consuming, and in some cases difficult to carry out. Therefore, concerning properties of the reacting system, thermodynamic and kinetic models are usually used as predictive tools to generate the required information. However, the accuracy and reliability of the used process simulation software depend on the performance of the predictive models implemented; validation, improvement or extension of which are anyway based first on the quality of the available experimental data (comprehensive databank with small experimental errors and good agreement between various literature sources). In other words, experimental information are essential for the development of predictive models, just as much as predictive and accurate models are essential for successful simulation and optimization of chemical processes **[13-14]**.

CHEMKIN II [15] and later releases, when associated with EXGAS [16], revealed to be very good candidate softwares for gas-phase chemical process simulation related to thermal cracking (pyrolysis and combustion) of various systems involving hydrocarbons [17-20] as well as oxygen containing species like ethers, alcohols and esters [2,21-24]. Besides the calculation techniques implemented in CHEMKIN II for simulating flow patterns in chemical reactors, the very good performances achieved are also due to two special features of EXGAS. First, EXGAS allows automatic generation of detailed kinetic mechanisms related to the investigated reacting systems (provided that all components can be handled by the implemented rules guiding the automatic generation). Secondly, EXGAS is based on a comprehensive and reliable databank of kinetic and thermophysical properties. Nevertheless, EXGAS has not been extended yet to thermal cracking reactions of $C_4^+$ carboxylic acids by lack of experimental information to validate the developed model (mechanism together with the associated kinetic and thermophysical properties).

As a result, the objective of this paper is to investigate the thermal decomposition of a large carboxylic acid and to present a new detailed kinetic model focused on octanoic acid pyrolysis together with the experimental data performed beforehand to validate the model. The latter was mainly generated by EXGAS, with some improvements brought for key reactions of which kinetic and thermophysical properties were estimated by quantum mechanics. The experimental data were generated by using a continuous tubular reactor close to plug flow in compliance with industrial reactors commonly found in pyrolysis, steam cracking or steam reforming processes. Moreover, from the modeling point of view, pyrolysis can be considered as the most basic thermal cracking reaction and octanoic acid as a good surrogate of biomass derived products, combining the COOH chemical function and a medium length carbon chain for a mechanism of manageable size. In addition, octanoic acid has been observed as major

product compound of bio-oils obtained by hydrothermal liquefaction of *Chlorella Vulgaris* biomass [11].

## 2.-Materials and methods

### *2.1. Experiment features*

Octanoic acid (OA > 99% pure, **Figure 1**) was provided by Acros Organics while nitrogen (99.995 pure) used in all experiments as inert diluent or carrier gas was provided by Air Liquide.

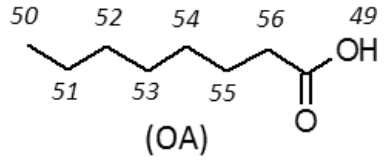


**Figure 1.** Molecular structure of octanoic acid (OA) and labels adopted for its C-H and O-H bonds.

A schematic layout of the bench-scale experimental setup used in this study is displayed in **Figure A1** (**Appendix A**). The core unit is a continuous tubular reactor in quartz (8 mm in inner diameter; 55 cm in length) very close to plug flow; this behavior was reached although the flow regime is laminar because the studied reaction occurs in gas-phase, leading to few axial dispersion (for the whole runs carried out, the mean values calculated for the key criteria are: Reynolds < 2300; Péclet ≥ 50). The tubular reactor (chemically treated to minimize surface effects) is housed in a thermostatically controlled oven (F 79300-type Thermolyne) ensuring a limited quasi-isothermal section. Hence, for a given oven set point, the reactor temperature profile is measured with a K-type thermocouple (100 cm length) that can be moved along the

central axis of the reactor. For avoiding surface catalytic reactions between the gas-phase and the thermocouple surface (in chromel/alumel), these temperature profiles were measured under pure nitrogen stream at molar flowrate close to that planned for pyrolysis experiments. The temperature profiles are displayed in **Figure 2** (and **Table B1**, **Appendix B**) for the oven set points corresponding to OA pyrolysis experiments. The operating pressure measured at the inlet of the reactor is considered as the operating pressure of the whole experimental setup.

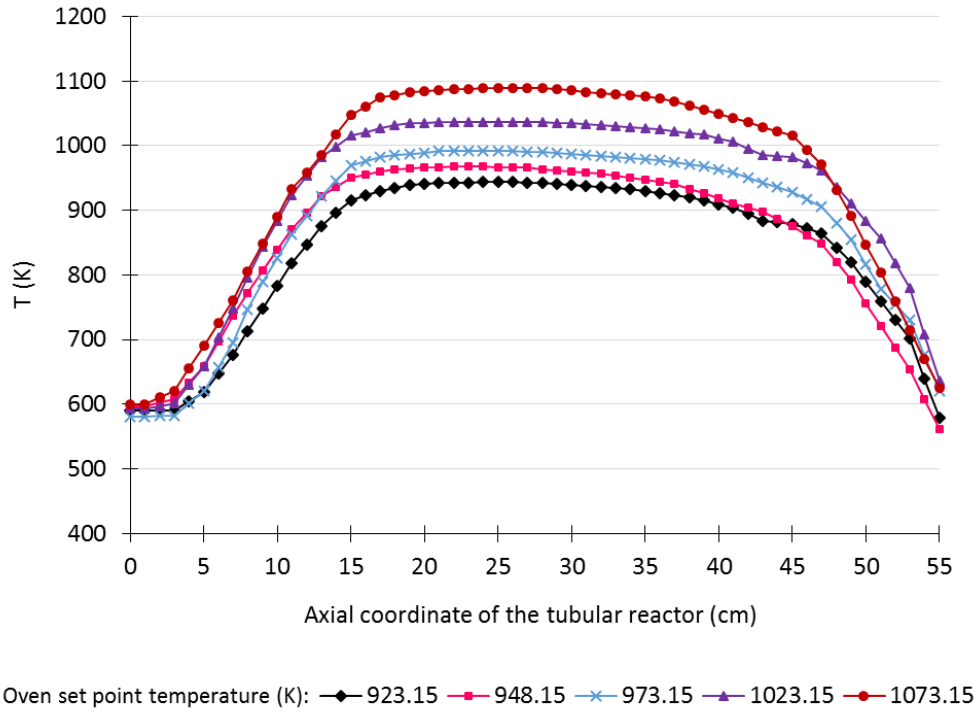


**Figure 2.** Experimental temperature profiles along the tubular reactor recorded for the different oven set point temperatures selected during the octanoic acid pyrolysis study.

Upstream of the reactor, a thermostatically controlled gas-liquid vaporizer (Pyrex vessel loaded with liquid OA in which a primary $N_2$ stream is bubbling counter-currently) allows for obtaining a homogenous gas reagent feed with a constant flowrate. Additionally to this OA/$N_2$ gas stream, a second $N_2$ stream is provided for conducting pyrolysis experiments at various dilutions of the reagent while maintaining constant the reagent feed residence time. Hence, both streams are mixed in an annular packed exchanger made in quartz and thermostatically

controlled. Although the two $N_2$ streams are controlled by mass flow controllers and maintained at constant temperature (around 573 K to avoid condensation and thermal cracking of octanoic acid), the exact molar flowrate of the reagent feeding the reactor is determined by operating without heating and collecting the reagent at the outlet of the reactor at equally space time intervals [25]. Next to the primary $N_2$ stream, an air supply is used at the end of each pyrolysis experiment to oxidize and quantify the coke formed during the run.

Downstream of the reactor, the reactant gas flow passes successively through a fast quenching, a condenser (both of them cooled down 293 K by a F30C-type Compact Julabo cryostat) and finally a gas-liquid separator for collecting the liquid products at the bottom while the gas products flowing out the top pass through a gas sampler for analysis and then an on-line gas flow meter.

Further details regarding this bench-scale experimental setup (design and material balance related equations, along with the operating procedure and the decoking step) are given in a previous work [25].

The pyrolysis products collected under three phases (gas, liquid, and solid when including coke) are analyzed by different techniques: *(i)* on-line non-dispersive infrared (NDIR) for CO and $CO_2$; *(ii)* on-line gas-chromatography (GC) equipped with a thermal conductivity detector (TCD) for $H_2$ and with a flame ionization detector (FID) for the $C_1$-$C_4$ gaseous species; *(iii)* off-line GC-FID for $C_4^+$ species. Calibration of the GC equipments used for non-condensable species was carried out with gas standard mixtures supplied by Air Liquide. After identification by GC-mass spectrometry by using the NIST database [26] (with at least 95% matching level for peak assignment and a visual comparison of species spectra), the condensable pyrolysis products together with the non-converted reagent (OA) were quantified by selecting two internal standards: n-dodecane for OA and n-octane for the other condensable products. Regarding alkenes and unsaturated carboxylic acids, pure compounds (provided by Sigma

Aldrich) were used to check the retention times and calibrate the GC-equipments. Details of GC equipments and operating conditions are displayed in **Table A1** (**Appendix A**). With this whole analysis equipment, mole fractions were determined with an accuracy of ± 5% for major species and ± 10% for minor species. Finally, coke deposit on the reactor internal surface has to be removed to satisfy material balances and to guarantee the reproducibility of the experiments. The amount of coke deposit was determined by burning it off and analyzing the resulting CO and $CO_2$ emissions by NDIR.

### *2.2. Modelling features for OA pyrolysis simulation*

#### *2.2.1. Tubular reactor model*

To take into account the temperature profile along the tube, the tubular reactor was modeled according to the Eulerian approach as a succession of perfectly stirred reactors using the PSR module of CHEMKIN II software **[15]**. The continuous tubular reactor assimilated rightly to a plug flow reactor (PFR) was thus modeled by a number of equivalent continuous stirred tank reactors (eCSTRs) in series $N_{eCSTRs}$, each uniform in composition, pressure, and temperature. The $N_{eCSTRs}$ value was set to 55 according to the number of measurements completed to define the temperature profile of the tubular reactor for a given oven set point (**Table B1**, **Appendix B**). Hence, each of these measurements being assigned to the temperature of each eCSTR, it is as though each eCSTR was located at an axial coordinate z of the tubular reactor, with z/cm ranging from 1 to 55 by step of 1 cm. Also, the residence time of the feed material along each eCSTR was considered identical for all and assigned to $\tau_{PFR}/N_{eCSTRs}$ , with $\tau_{PFR}$ the residence time of the feed material along the tubular reactor. Assumptions used by this modelling led minimal effects; assigning $N_{eCSTRs}$ to a higher value

proved not affect pyrolysis simulation results; the major errors over residence time are made for the eCSTRs operating at the lower temperatures, i.e. where no reaction occurs.

*2.2.2. Kinetic model*

The automatic generation of detailed kinetic mechanisms with the required kinetic and thermodynamic data as obtained by the EXGAS version used in this work (i.e. with extension to oxygenated species except carboxylic acids) have already been described in the literature **[2,21-24]**. Therefore, only the main features are briefly recalled in **Appendix C** **[15-16, 27-28]**. In order to take into account the specific chemistry of carboxylic acids, some changes had to be made in both the primary mechanism, devoted to the consumption of the reactant and its resulting radicals, and in the secondary mechanism devoted to the consumption of the stable species produced from the primary mechanism (**Appendix C**). These changes listed in **Table C1** concern both supplementary reactions and new estimations of kinetic and thermodynamic data on the basis of the literature or quantum calculations carried out in this work. The most significant changes are briefly commented in the following.

Regarding the primary mechanism, the two competing molecular eliminations of OA, i.e decarboxylation and dehydration leading respectively to the formation of n-heptane and hexylketene, were accounted with the rate constants proposed by Clark et al. **[29]**. As OA is an acid with α-hydrogens, dehydration may proceed either through a concerted 4-membered reaction or through a two-step process with an 1,1-enediol intermediate. For this second reaction pathway, formation and dehydration of 1,1-enediol were shunted in this work into one single reaction by affecting to it the rate constant of the 1,1-enediol formation limiting step. The thermodynamic properties of hexylketene ($C_6H_{13}CH=C=O$) were determined by Benson's group contribution method **[27]** completed with Sumathi and Green's data based on quantum calculations **[42]**. H-atom abstractions are among the most sensitive reactions in pyrolysis. Rate

constants of the abstraction of the acid H-atoms and of H-atoms in α−position of the carboxyl group were estimated based on correlations from the literature and analogies with similar reactive sites (**Table C1a**). Rate constants of C-H bond β-scissions for OA radicals leading to α,β or β,γ-unsaturated carboxylic acids were revisited. The kinetic parameters of these reactions were estimated from an Evans Polanyi plot based on theoretical calculation for reactions of alkyl radicals [36]. A lower activation energy was obtained for the reaction leading to α,β-unsaturated carboxylic acids due to their chemical structure stabilized by π-electrons delocalization (**Table C1a**).

Regarding the secondary mechanism, sub-mechanisms of formic and acetic acids proposed by Sun et al. [32] were introduced with some improvements. For acetic acid, kinetic parameters of the enediol formation were changed for those proposed by Clark et al. [29] in order to get a better agreement with experiments. Still for this reaction, Cavallotti et al. [39] also observed a large discrepancy between their rate calculations and those proposed by Sun et al. [32], but a good agreement with those obtained by Clark et al. [29]. Moreover, the thermodynamic properties of $^{\bullet}CO_2H$ and $HCOO^{\bullet}$ radicals together with formic acid were determined from Marshall and Glarburg [43], while Sun et al. [32] estimations were kept for acetate radical $CH_3COO^{\bullet}$.

The isomerization of $^{\bullet}CH_2COOH$ to $CH_3COO^{\bullet}$ by a H-transfer via a four centered transition state together with the decomposition of $^{\bullet}CH_2COOH$ into $CH_2=C=O$ and $^{\bullet}OH$ by β-scission of the C-O bond were also included. Sun et al. [32], nor the previous kinetic models of acetic acid combustion, have taken this isomerization into account. This lack led authors to propose unrealistic rate constant for the decomposition of $^{\bullet}CH_2COOH$ radical into ketene, with an activation energy far below reaction endothermicity. Beside, this lack gives a physical explanation to Leplat and Vandooren [44] requirement of dividing by 2 the energy activation proposed by Gasnot et al. [45] for $^{\bullet}CH_2COOH$ decomposition in order to prevent the radical

reacting back to $CH_3COOH$. In this work, the rate constants of these two reactions were determined by *ab initio* calculations at the CBS-QB3 level of theory, with a methodology described elsewhere **[46]**. Usually, the CBS-QB3 level of theory provides estimations with ± 2 kcal·mol$^{-1}$ on the activation energy and a factor 2 on the exponential factor. The isomerization was found to be much easier than the decomposition to ketene, with energy barriers at 0 K of 41.7 kcal·mol$^{-1}$ and 52.5 kcal·mol$^{-1}$, respectively. The produced $CH_3COO^{\bullet}$ radical decomposes then very fast to $CO_2$ and a methyl radical. The high pressure rate constant $k_\infty$ was determined thank to the transition state theory and fitted in the range of 500 to 1700 K.

Two additional classes of reactions were implemented to account for consumption of monounsaturated carboxylic acids; produced mainly by β-scission of radicals from OA, the ethylenic bond is located at the opposite aliphatic extremity from the carboxylic group. The first class is the $^{\bullet}H$ and $^{\bullet}CH_3$ additions on the $CH_2$=CH- bond. While the $^{\bullet}H$ addition leads to saturated acid radicals with invariant carbon number, the $^{\bullet}CH_3$ addition leads after a subsequent β-scission to two shorter species: an alkene and a saturated acid radical (**Table C1b**). The second class of reactions is the retro-ene decomposition of $C_6$ to $C_8$ acids yielding two shorter unsaturated molecular species through a six-centered transition state: an alkene and an unsaturated acid (**Table C1b**). All kinetic parameters of these two classes of reactions were taken from the work on alkene oxidation by Touchard et al. **[41]**.

Furthermore, the Arrhenius pre-exponential factor for combination of radicals $^{\bullet}CH_2COOH$ and $^{\bullet}C_2H_5$ to form $C_3H_7COOH$ was set to $10^{12}$ in accordance with similar reactions of large alkyl radicals **[37]** for a good agreement with experiments.

The obtained kinetic model (detailed kinetic mechanism involving 218 species and 1416 reactions, together with the corresponding kinetic and thermodynamic data) is available as Supporting Information (SI).

## 3.-Results and discussion

### *3.1. Experimental data generated and major pyrolysis products observed*

The three reaction parameters selected for their influence on the chemical nature and amount of the pyrolysis products are: reaction temperature, residence time of the feed material, and extent of dilution of the reactant (OA).

The detailed experimental data generated during OA pyrolysis in PFR are listed in **Tables B2-B4** (**Appendix B**). The selected operating conditions are: for the oven set point temperature, from 923 to 1073 ± 1 K; for the reactor pressure, 112 ± 4 kPa; for the mean residence time, from 421 ± 13 to 826 ± 21 ms; for OA mole fraction in $N_2$, 3 and 5%. For each run, the mean residence time was determined by considering the reactor pressure and the reactor mean temperature (average of the reactor temperature profile values recorded for a given oven set point; **Table B1**, **Appendix B**). Among all the experiments carried out, only those with satisfactory errors in overall material balance (< 0.05% in mass) and acceptable errors in C-H-O element mole balances (≤ 6% in mole for C and H) were retained. Selecting such criteria to reject experiments containing errors (these being mainly induced when weighing the collected liquid product or when carrying out the GC analyses to identify/quantify the formed species) revealed to be appropriate in the previously published works **[6,24]**. Larger deviations in oxygen mole balance were observed very likely because some species containing O atom could not be quantified properly (specifically water, formaldehyde, and ethenone). Repeatability evaluated by duplicating one set of operating conditions (exp. 7 and exp. 8) led to rather good results (coefficient of variation < 10%, with the exception of CO mole fraction observed in the low limit of detection of the NDIR analyzer used; **Table B5** **[25]**, **Appendix B**).

Within the operating conditions selected in this work, the major chemical species identified as products from OA pyrolysis are: *(i)* $C_1$-$C_4$ hydrocarbons, i.e. methane, acetylene, ethane, propane, and 1,3-butadiene; *(ii)* $C_2$-$C_7$ 1-olefins, i.e. ethylene, propene, 1-butene, 1-pentene, 1-hexene, and 1-heptene; *(iii)* $C_2$-$C_7$ carboxylic acids (saturated and homologous monounsaturated species with the ethylenic bond located at the opposite aliphatic chain extremity from the carboxylic group) i.e. acetic, propenoic, propanoic, 4-pentenoic, pentanoic, 5-hexenoic, hexanoic, 6-heptenoic, and heptanoic acids; *(iv)* carbon monoxide, carbon dioxide, hydrogen, and coke. Butanoic and 7-heptenoic acids were not observed experimentally because their mole fractions were below the detection limit of the GC-FID used. By contrast, 3-butenoic acid should have been quantified significantly but was neither observed very likely because of overlapping with another species.

### *3.2. Reaction flux and sensitivity analyses from the developed kinetic model*

A reaction flux analysis based on species consumption rate calculation was carried out in order to get the main routes of OA decomposition and of formation of pyrolysis products and intermediates. In order to highlight the most important reaction pathways, this reaction flux analysis was completed with a sensitivity analysis based on calculation of normalized sensitivity coefficients of OA mole fractions with respect to reaction rates. A negative (positive) sensitivity coefficient indicates that an increase in the reaction rate implies a decrease (increase) of the OA mole fraction, meaning that this reaction promotes (inhibits) reactivity. Both analyses (performed via the PSR module of CHEMKIN II **[15]**) were carried out under the same experimental conditions (1 atm and 1087 K, for 421 ms residence time and 5% molar OA in $N_2$), with two additional residence times for the sensitivity analysis (616 and 826 ms). Results

are reported in **Figure 3** for the reaction flux analysis and in **Figure 4** for the sensitivity analysis (overall decomposition scheme depicted by **Figure D1**, **Appendix D**).

As it can be observed, under the experimental conditions selected, OA decomposes mainly by H-abstractions on the aliphatic chain (82%) with a major contribution leading to the α-radical $\dot{R}_{56}$ (14%, which also reveals the most sensitive reaction increasing OA consumption) and a lower contribution to the radical $\dot{R}_{50}$ carrying the unpaired electron at the opposite aliphatic extremity from the carboxylic group (7%). The lowest part of OA decomposition by H-abstraction is from the acid hydrogen of the carboxylic group (2%), which reveals to be not easy to abstract; the resulting radical $\dot{R}_{49}$ entirely yields heptyl radical with release of one $CO_2$ molecule. A more straightforward reaction pathway leading to $CO_2$ release is the OA decarboxylation with n-heptane formation that competes almost equally with the other OA molecular elimination path, i.e. dehydration with formation of hexylketene (3 and 4% of OA consumption, respectively). A branching ratio $[H_2O]/[CO_2]$ close to unity was also observed by Clark et al. **[29]** for saturated carboxylic acids. While the unimolecular decomposition reactions appear to consume OA with a lower extent (6% for the whole of them), these are among the most sensitive promoting reactions, particularly when residence time increases. Moreover, **Figure 3** and **Figure D1** show clearly that all products observed experimentally are formed in the mechanism. Products in larger amounts are the small species ($H_2$, CO, $CO_2$, methane, including carboxylic acids and 1-olefins with 2 to 4 carbon atoms) formed in many significant production flows. Also, **Figure 4** highlights two important features. First, H-abstraction reactivity of OA strongly increases with residence time (on average, sensitivity coefficients are multiplied by 1.7 when τ changes from 421 to 826 ms). Secondly, residence time has also a significant impact on most of the combination reactions which drop off OA reactivity by removing from the radical pool the most reactive species $^{\bullet}H$ and $^{\bullet}CH_3$.

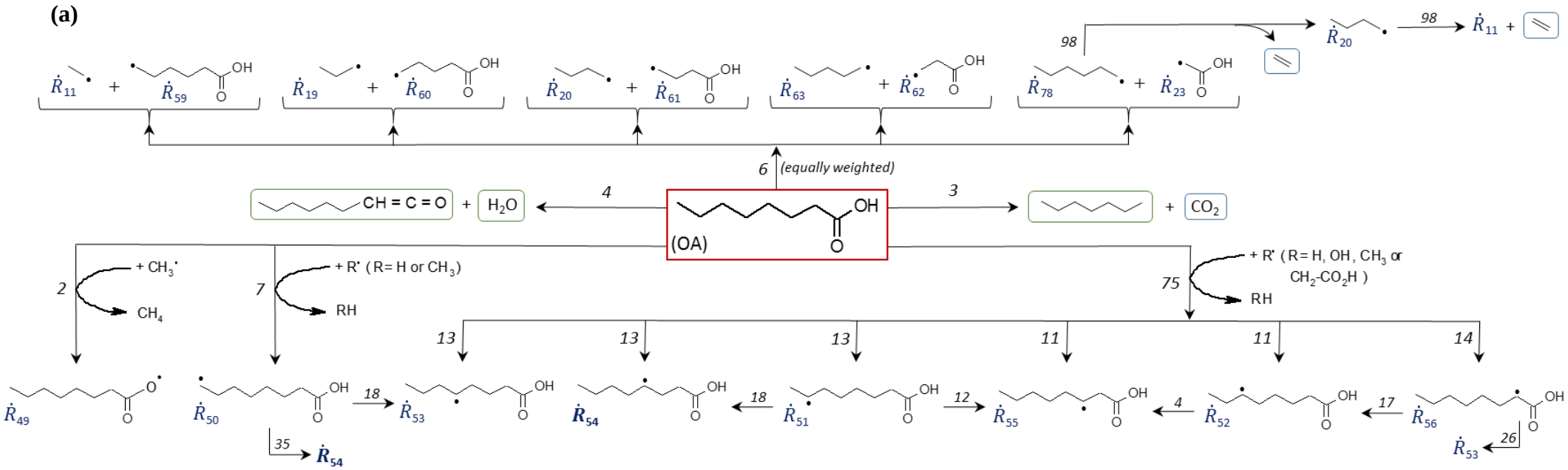


**Figure 3.** Decomposition of octanoic acid (OA) at 1 atm and 1087 K for 421 ms residence time and 5% molar OA in $N_2$ (oven set point temperature: 1073.15 K; PFR axial coordinate: 22 cm; 30% conversion of OA); **(a)** H-abstractions and unimolecular reactions leading to OA radicals ($\dot{R}_{49}$ to $\dot{R}_{56}$); **(b)** Main decomposition paths of OA radicals $\dot{R}_{49}$, $\dot{R}_{50}$, $\dot{R}_{51}$, $\dot{R}_{52}$, $\dot{R}_{53}$, and $\dot{R}_{54}$; **(c)** Main decomposition paths of OA radicals $\dot{R}_{52}$, $\dot{R}_{55}$, and $\dot{R}_{56}$. Italic numbers indicate percent of parent species being converted to daughter species. C5H8O2ZB, C6H10O2ZB and C8H14O2ZB are globalized species taking into account isomers from which the major forms are respectively: $CH_2$=CH-$CH_2$-$CH_2$-COOH, $CH_2$=CH-$(CH_2)_3$-COOH, and $CH_2$=CH-$(CH_2)_3$-COOH.

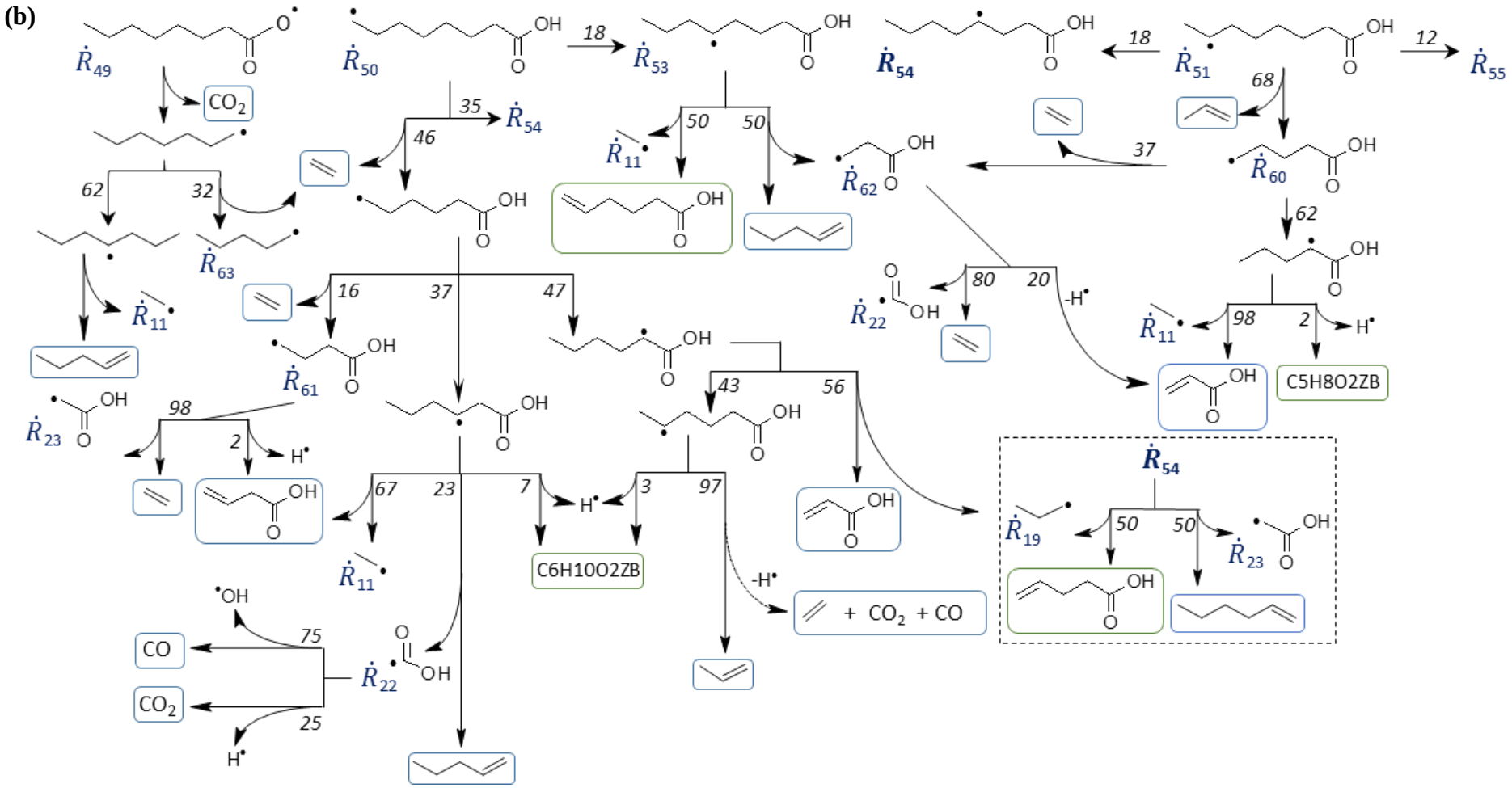


**Figure 3.** Continued.

**(c)**

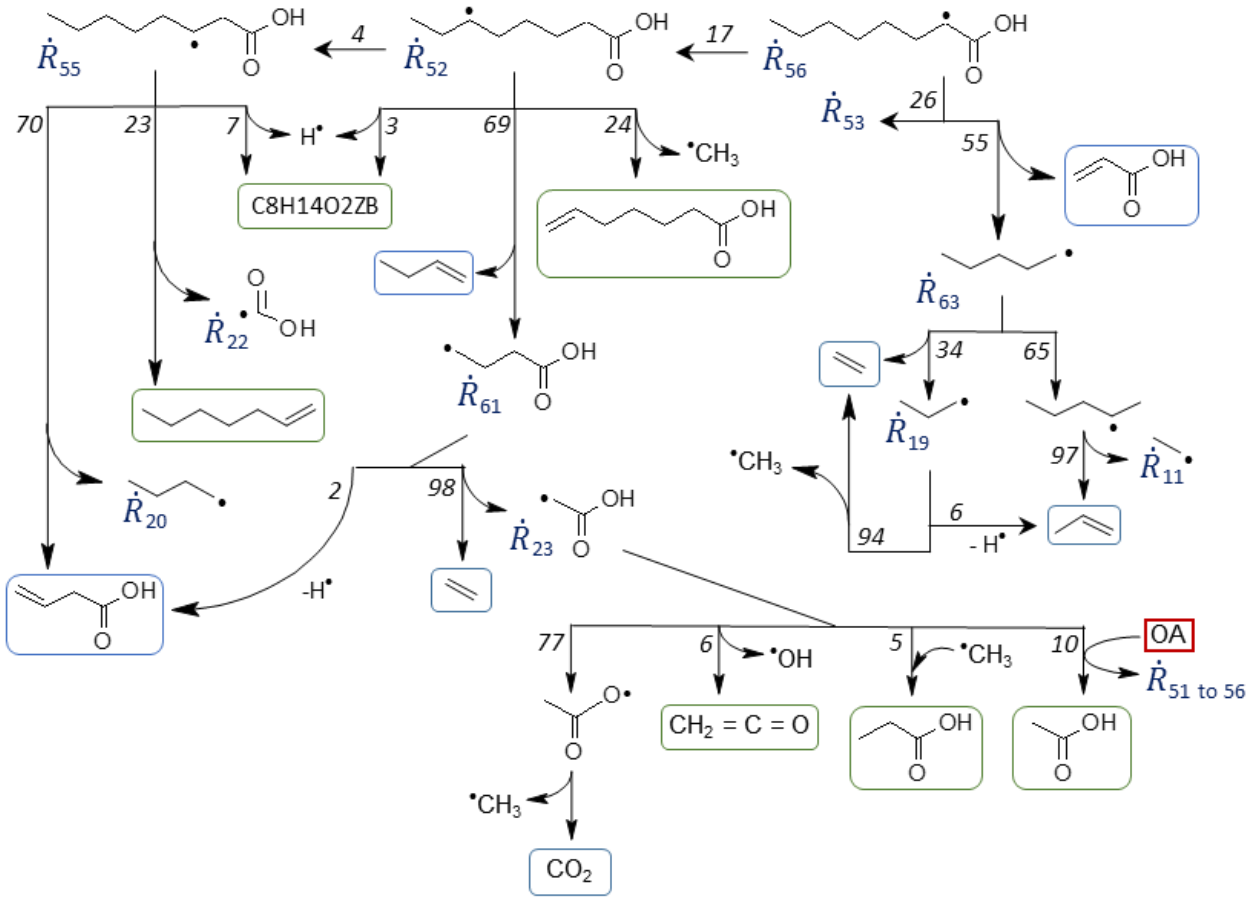


**Figure 3.** Continued.

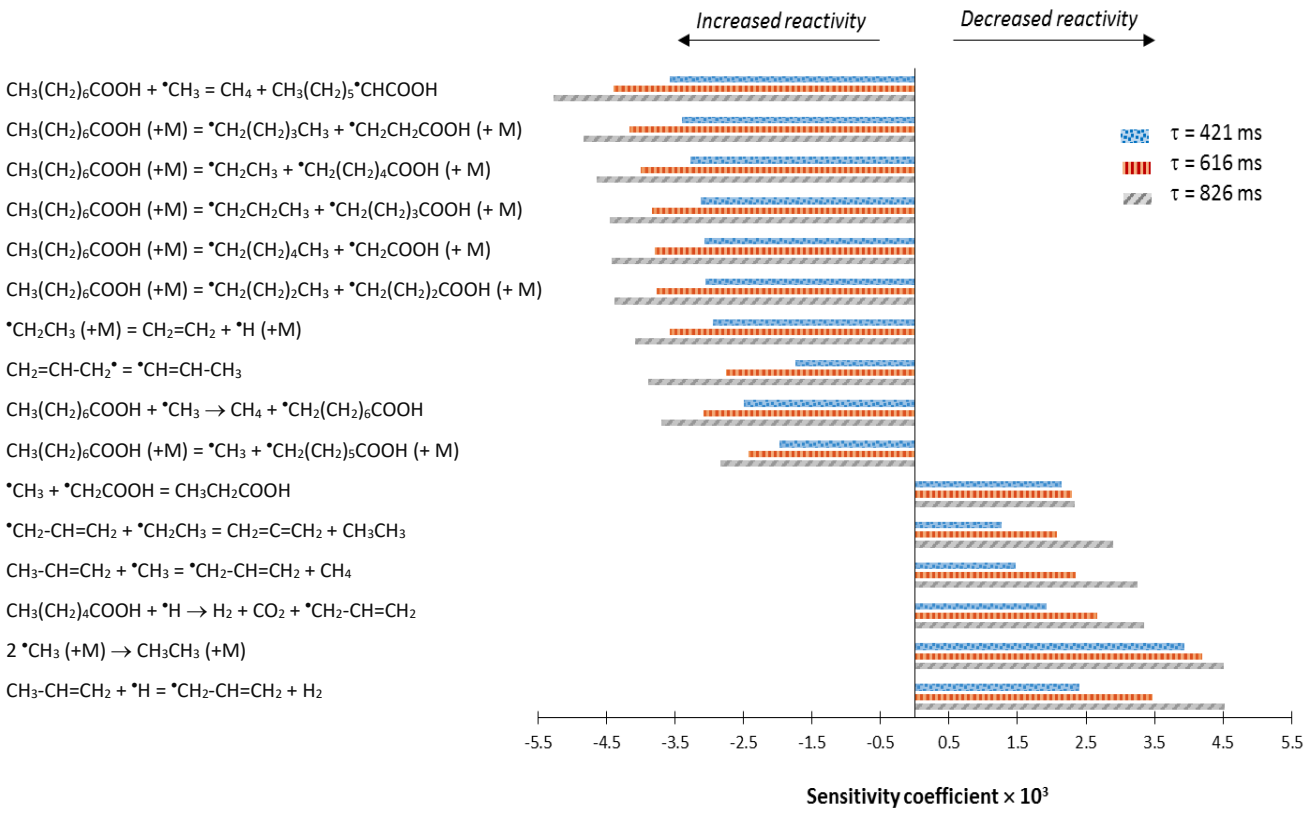


**Figure 4.** Normalized sensitivity coefficients for 5% molar octanoic acid (OA) in nitrogen at 1 atm and 1087 K, for three mean residence times: 421, 616, and 826 ms (oven set point temperature: 1075.15 K; axial coordinate of the tubular reactor: 22 cm), with OA selected as sensitivity target.

### *3.3. Modeling performance in terms of pyrolysis temperature, residence time and reactant dilution*

Quantitative comparison between experimental and modeling results is depicted in **Figure 5** for the highest OA mole fraction (5%) while the impact of the OA dilution is shown in **Figure E1** (**Appendix E**) for the lowest residence time (421 ms). The conversion of OA reaches a maximum of 45% within the investigated ranges of reaction temperature and

residence time (**Table B4, Appendix B**). Hence, the experimental data will be exploitable to validate the primary mechanism of OA pyrolysis occurring at very low conversion (inferior than 10%) as well as the secondary mechanism (taking place at higher conversion).

As it could be expected, OA conversion increases with pyrolysis temperature and residence time. Regarding pyrolysis products, the species profiles confirm that an increase in reaction temperature or in residence time promotes the production of small species such as $H_2$, CO and $CO_2$, but also light 1-olefins and carboxylic acids ($C_2$-$C_4$ species), besides methane, ethane, and 1,3-butadiene (**Figures 5**). Indeed, $H_2$, CO, $CO_2$, methane, ethylene, and propene deriving from thermal decomposition of both of the reactant and products (**Figure 3**), are then formed in large amounts. Nevertheless, it should be noticed that CO and $CO_2$ mole fractions start to be significant only beyond 1000 K, revealing a very slow reactivity for the carboxylic acid group at low temperature (below 925 K).

Furthermore, pyrolysis temperature and residence time enhance also formation of heavier 1-olefins ($C_5$-$C_7$ species) but only up to 1000 K. Beyond this temperature, mole fraction of these species decreases to become zero from 1075 K. It is valuable to notice that at 1025 K, the lowest level of heavy 1-olefins is observed for the longest residence time. Hence, starting from this temperature (1025 K), heavy 1-olefins decompose thermally into smaller molecules, and this, with a level all the more high that residence time is long. Besides, this result explains the steadily increasing mole fractions of methane, ethane, ethylene, and propene with pyrolysis temperature and residence time. Indeed, enhanced conversion of OA promotes secondary reactions of heavy 1-olefins (primary products) producing then ethylene and propene by successive β-scissions while yielding methyl radical ($^{\bullet}CH_3$) which in turn reacts very fast to form methane by H-abstraction.

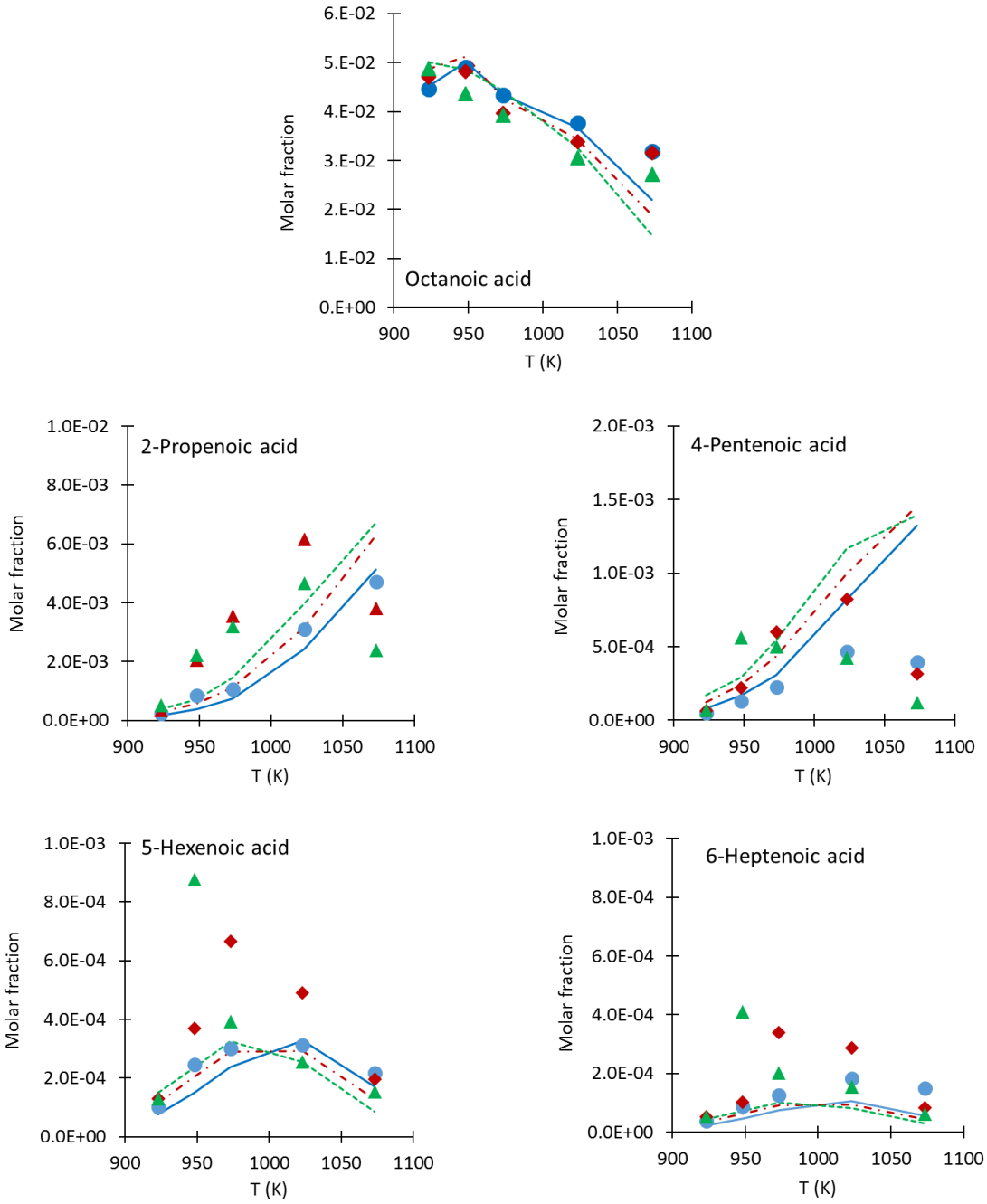


**Figure 5.** Reactant and product mole fraction profiles *vs.* temperature resulting from octanoic acid pyrolysis carried out in a plug flow reactor at 1 atm for various residence times of the feed material (mixture of 5.0% molar octanoic acid in $N_2$). Symbols are experimental results and lines are model simulations, with different colors to differentiate the residence times: 421 ms (blue), 616 ms (red), 826 ms (green). Butanoic acid, 3-butenoic acid, and 7-octenoic acid were not observed experimentally, and thus were not plotted; as well propanoic acid and propane which were detected only near 1075 K and 826 ms with a mole fraction of 0.05 and 0.02% respectively.

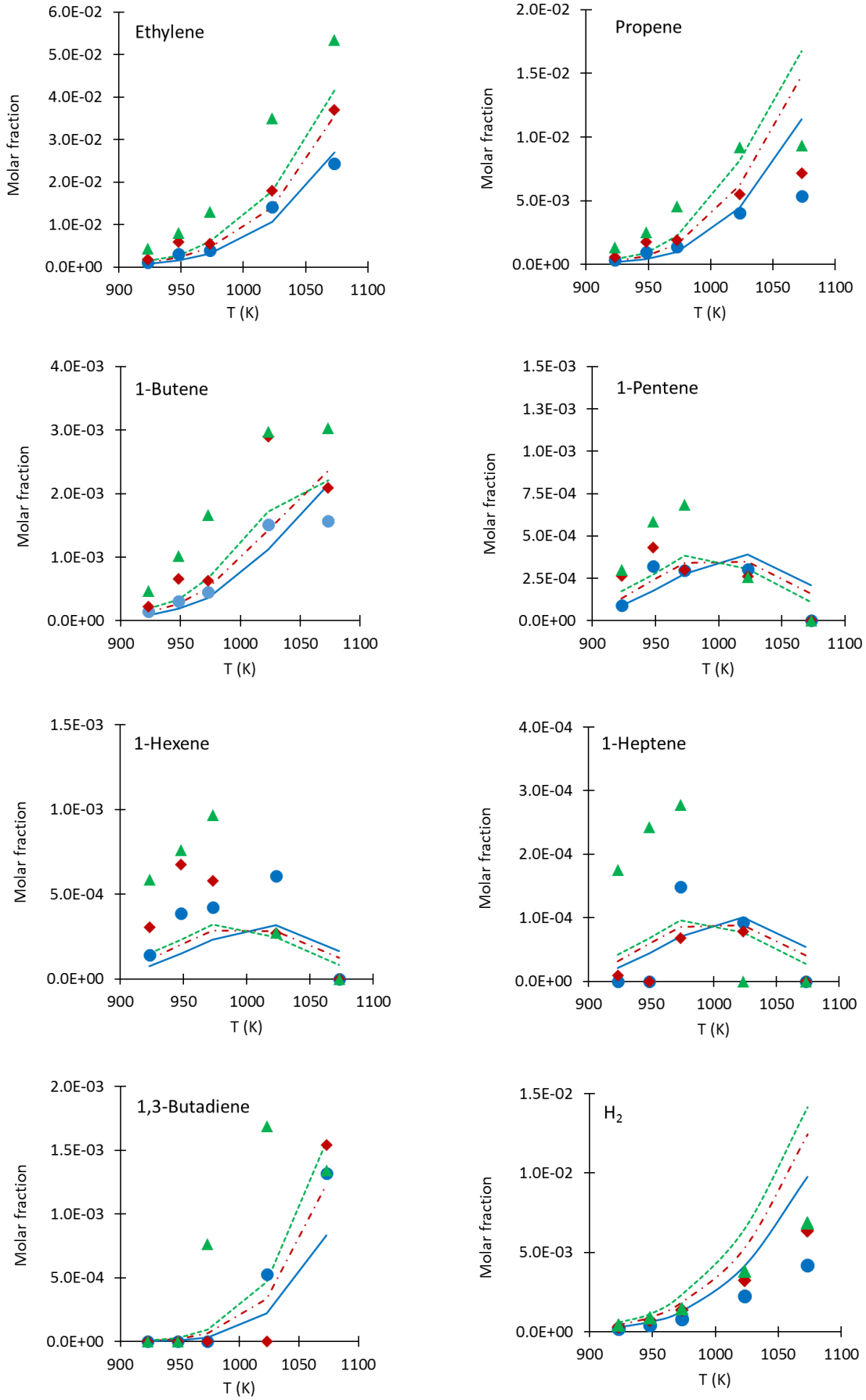


**Figure 5.** Continued.

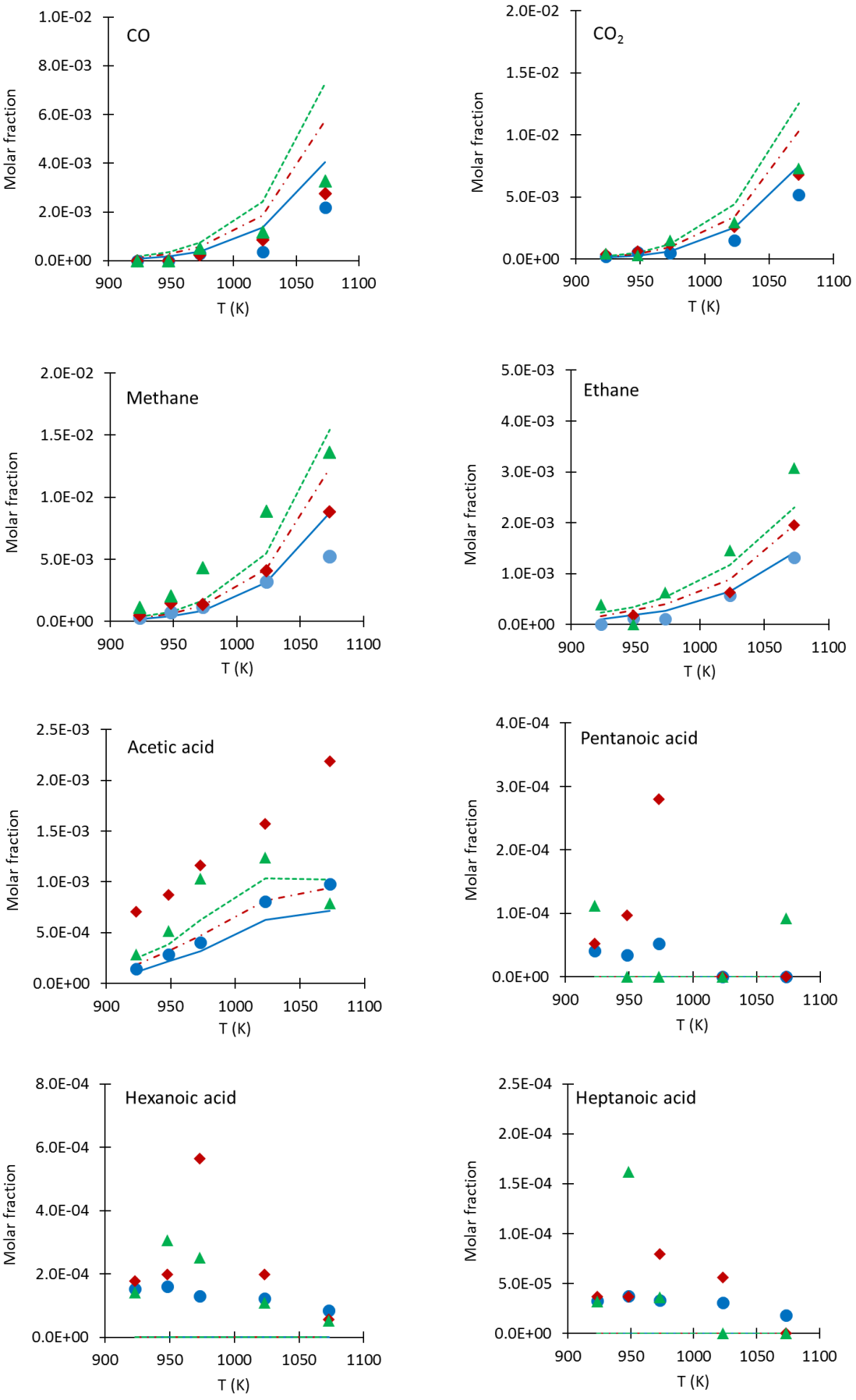


**Figure 5.** Continued.

Another significant fact clearly showed in **Figure 5** is that mole fractions of $C_5$-$C_7$ monounsaturated carboxylic acids follow exactly the same progression with temperature and residence time than mole fractions of $C_5$-$C_7$ 1-olefins, i.e. an increase up to a limit temperature (1025 K) and then, a decrease all the more sharp than the residence time increases. This result confirms that, within the primary mechanism, the OA radicals ($\dot{R}_{50}$ to $\dot{R}_{56}$, **Figure 3**) decompose to produce symmetrically either monounsaturated carboxylic acids (together with alkyl radicals) or 1-olefins (together with carboxyalkyl radicals). Thereafter, monounsaturated carboxylic acids are consumed at high temperature through radical paths of the secondary mechanism to yield mainly short 1-olefins ($C_2$-$C_4$ species), 1,3-butadiene, CO, $CO_2$, and $H_2$, but also smaller saturated carboxylic acids ($C_2$-$C_4$ species). Therefore this last class of products (together with short 1-olefins) has mole fractions steadily increasing with pyrolysis temperature and residence time (**Figure 5**). By contrast, mole fractions of heavier saturated carboxylic acids ($C_5$-$C_7$ species) increase up to a limit temperature (1000 K) and then decrease (**Figure 5**), similarly to their unsaturated homologous species. Besides, as illustrated in **Figure 3**, the saturated carboxylic acids are produced from carboxyalkyl radicals ($\dot{R}_{59}$ to $\dot{R}_{62}$, and $\dot{R}_{23}$ coming from OA unimolecular decomposition) which can then react by H-abstraction from the reactant OA and a fewer extent by combination with H atom. Note that with the resonance stabilized $^{\bullet}CH_2COOH$ radical ($\dot{R}_{23}$), the molecular species formed $CH_3COOH$ is very stable in gas phase, which explains why acetic acid is the major component among the saturated acids (**Figure 5**). Thus, as confirmed by **Figures 4** and **5,** formations of 1-olefins and saturated carboxylic acids are closely linked and the mole fractions of these species as function of pyrolysis temperature or residence time show very similar progressions.

In accordance with previous observations, **Figure 5** shows that the proposed kinetic model is able to depict well the reactivity of OA, including the amounts of the small species

$H_2$, CO, $CO_2$, methane, ethane, ethylene, and propene, which are among the most abundant products. The largest deviations are observed for the highest temperature and longest residence time, for which the kinetic model overestimates OA conversion and consequently, the production of these small species too. Nevertheless, the kinetic model renders properly the specific shape of the profiles observed for the heavy $C_5$-$C_7$ alkenes, considering the dispersion of the experimental data. The species that are the most poorly described are saturated carboxylic acids, including acetic acid that is produced experimentally in rather significant amounts. Note that the model does not predict the drop of the acetic acid fraction at the longest residence time which may due to experimental uncertainties or to the omission of reaction pathways. A similar disagreement between experiments and modelling was observed by Namysl et al. **[47]** regarding pentanoic acid oxidation. In this work, saturated carboxylic acids up to C7 were included in the mechanism. The main formation pathways are H-atom abstractions from OA by carboxyalkyl radicals $^{\bullet}$RCOOH (reactions 2b in **Table C1, Appendix C**). This unique channel cannot take into account the amount of carboxylic acids produced while keeping realistic kinetic parameters. Existence of hydrogen bonds connecting two carboxylic acid units with a rather strong energy (60 kJ·mol$^{-1}$) leads to associated bi-molecules observable in gas-phase **[48]**. Hydrogen bond associations may also induce wall effects and cross hydrogen associations between oxygen species which impact their analysis. Hence, such hydrogen bond associations alter somewhat the thermal decomposition of carboxylic acids **[49]** and the omission of this effect in the modelling may explain partly the deviations observed for these species. Lastly, increasing the OA reactant dilution improves the kinetic model agreement with experiments, for all conditions of temperature and residence time investigated and all classes of products, including the reactant OA.

## 4. Conclusion

The experimental data generated in this work with a plug flow reactor were of precious help to develop a detailed kinetic model for octanoic acid pyrolysis. Within the selected operating conditions of the plug flow reactor (atmospheric pressure with an oven temperature ranging from 923-1073 K) the major products formed are 1-olefins and carboxylic acids (saturated and monounsaturated) together with small species like hydrogen, carbon monoxide, carbon dioxide, methane and ethylene. Although mainly generated by EXGAS software, the model required some improvements to take into account the specific reactivity of the carboxylic group (additional reactions implemented with thermodynamic and kinetic properties). A rather satisfactory agreement with the experiments was observed for octanoic acid and the major small pyrolysis products ($H_2$, CO, $CO_2$, methane, and ethylene). The specific trend of the alkene profiles was satisfactorily reproduced by the model too. Nevertheless, some deviations still remain, particularly for saturated carboxylic acids. Additional information on pyrolysis for this class of molecules would improve the understanding of the physical-chemical specificity of the carboxylic group on their thermal reactivity.

## Appendices A-E. Supplementary data

Supplementary material related to this article (**Appendices A-E**) can be found, in the online version. Proposed chemical kinetic reaction mechanism and associated thermochemical data, all in CHEMKIN format, are also available.

## References

[1] Zhang Y., Yang Y., Boehman A.L. Premixed Ignition Behavior of C9 Fatty Acid Esters: a Motored Engine Study, Combust. Flame 156 (2009) 1202-1213.

[2] Hakka, M.H., Bennadji, H., Biet, J., Yahyaoui, M., Sirjean, B., Warth, V., Coniglio, L., Herbinet, O., Glaude, P. A., Billaud, F., Battin-Leclerc, F. Oxidation of Methyl and Ethyl Butanoates, Int. J. Chem. Kinet. 42 (2010) 226-252.

[3] Cosseron, A.F., Bennadji, H., Leyssens, G., Coniglio, L., Daou, T.J., Tschamber, V. Evaluation and Treatment of Carbonyl Compounds and Fine Particles Emitted by Combustion of Biodiesels in a Generator, Energy Fuels 26 (2012) 6160-6157.

[4] Coniglio, L., Coutinho, J.A.P., Clavier, J.Y., Jolibert, F., Jose, J., Mokbel, I., Pillot, D., Pons, M.N., Sergent, M., Tschamber, V. Biodiesel via Supercritical Ethanolysis within a Global Analysis "Feedstocks-Conversion-Engine" for a Sustainable Fuel Alternative, Prog. Energy Combust. Sci. 43 (2014) 1-35.

[5] Choe, E., Min, D.B. Chemistry of Deep-Fat Frying Oils, J. Food Sci. 72 (2007) 77-78.

[6] Gornay, J., Coniglio, L., Billaud, F., Wild, G. Steam Cracking and Steam Reforming of Waste Cooking Oil in a Tubular Stainless Steel Reactor with Wall Effects, Energy Fuels 23 (2009) 5663-5676.

[7] Mohan, D., Pittman, C.U., Steele, P.H. Pyrolysis of Wood/Biomass for Bio-oil: A Critical Review, Energy Fuels 20 (2006) 848-889.

[8] Ferrando, N., Gedik, I., Lachet, V., Pigeon, L., Lugo, R. Prediction of Phase Equilibrium and Hydration Free Energy of Carboxylic Acids by Monte Carlo Simulations, J. Phys. Chem. B 117 (2013) 7123-7132.

[9] Brillouet, S., Baltag, E., Brunet, S., Richard, F. Deoxygenation of Decanoic Acid and its Main Intermediates over Unpromoted and Promoted Sulfided catalysts, Appl. Catal. B-Environ. 148-149 (2014) 201-211.

[10] Fu, J., Lu, X., Savage, P.E. Hydrothermal Decarboxylation and Hydrogenation of Fatty Acids Over Pt/C, ChemSusChem 4 (2011) 481-486.

[11] Gollakota, A.R.K., Kishore, N., Gu, S. A Review on Hydrothermal Liquefaction of Biomass, Renew. Sust. Energ. Rev. 81 (2018) 1378-1392.

[12] Asomaning, J., Mussone, P., Bressler, D.C. Thermal Deoxygenation and Pyrolysis of Oleic Acid, J. Anal. Appl. Pyrolysis 105 (2014) 1-7.

[13] Diaz-Tovar, C.A., Gani, R., Sarup, B. Lipid Technology: Property Prediction and Process Design/Analysis in the Edible Oil and Biodiesel Industries, Fluid Ph. Equilibria 302 (2011) 284-293.

[14] Anjan Kumar Tula, A.K., Eden, M.R., Gani, R. Process Synthesis, Design and Analysis using a Process-Group Contribution Method, Comp. Chem. Eng. 81 (2015) 245–259.

[15] Kee, R. J., Rupley, F. M., Miller, J. A. Chemkin II. A Fortran Chemical Kinetics Package for the Analysis of a Gas-Phase Chemical Kinetics. Sandia Laboratories Report, SAND 89-8009B, 1993.

[16] Warth, V., Stef, N., Glaude, P.A., Battin-Leclerc, F., Scacchi, G., Côme, G.M. Computer-Aided Derivation of Gas-Phase Oxidation Mechanisms: Application to the Modelling of the Oxidation of n-Butane, Combust. Flame 114 (1998) 81-102.

[17] Dahm, K.D., Virk, P. S., Bounaceur, R., Battin-Leclerc, F., Marquaire, P. M., Fournet, R., Daniau, E., Bouchez, M. Experimental and Modelling Investigation of the Thermal Decomposition of n-Dodecane, J. Anal. Appl. Pyrol. 71 (2004) 865-881.

[18] Buda, F., Bounaceur, R., Warth, V., Glaude, P. A., Fournet, R., Battin-Leclerc, F. Progress Toward a Unified Detailed Kinetic Model for the Autoignition of Alkanes from C4 to C10 Between 600 and 1200 K, Combust. Flame 142 (2005) 170-186.

[19] Vanhove, G., Minetti, R., Touchard, S., Fournet, R., Glaude, P.A., Battin-Leclerc, F. Experimental and Modelling Study of the Autoignition of 1-Hexene / Iso-octane Mixtures at Low Temperature, Combust. Flame 145 (2006) 272-281.

[20] Biet, J., Hakka, M.H., Warth, V., Glaude, P.A., Battin-Leclerc, F. Experimental and Modelling Study of the Low-Temperature Oxidation of Large Alkanes, Energy Fuels 22 (2008) 2258-2269.

[21] Glaude, P. A., Battin-Leclerc, F., Judenherc, B., Warth, V., Fournet, R., Côme, G. M., Scacchi, G., Dagaut, P., Cathonnet, M. Experimental and Modelling Study of the Gas-Phase Oxidation of Methyl and Ethyl-tert-Butyl Ethers, Combust. Flame 121 (2000) 345-355.

[22] Moss, J. T., Berkowitz, M., Oehlschlaeger, M. A., Biet, J., Warth, V., Glaude, P. A., Battin-Leclerc, F. An Experimental and Kinetic Modelling Study of the Oxidation of the Four Isomers of Butanol, J. Phys. Chem. A 112 (2008) 10843-10855.

[23] Glaude, P.A., Herbinet, O., Bax, S., Biet, J., Warth, V., Battin-Leclerc, F. Modelling of the Oxidation of Methyl Esters – Validation for Methyl Hexanoate, Methyl Heptanoate, and Methyl Decanoate in a Jet-Stirred Rector, Combust. Flame 127 (2010) 2035-2050.

[24] Bennadji, H., Glaude, P.A., Coniglio, L., Billaud, F. Experimental and Kinetic Modelling Study of Ethyl Butanoate Oxidation in a Laminar Tubular Plug Flow Reactor, Fuel 90 (2011) 3237-3253.

[25] Gornay, J., Plasari, E., Glaude, P.A., Billaud, F., Coniglio, L. How to Design a Bench-Scale Tubular Reactor Close to Plug Flow Reactor for Gas-Phase Kinetic Data Generation? Case Study of Octanoic Acid Pyrolysis, J. Anal. Appl. Pyrol. (2019) under process submission.

[26] NIST Mass Spectrometry Data Center. NIST MS number 236029. Retrieved from: http://webbook.nist.gov. Last major update to the site: 9 February 9 2015.

[27] Benson, SW., Thermochemical kinetics. 2nd ed. New York: John Wiley; 1976.

[28] Muller, C., Michel, V., Scacchi, G., Côme, G.M. A Computer Program for the Evaluation of Thermochemical Data of Molecules and Free Radicals in the Gas Phase, J. Chem. Phys. 92 (1995) 1154-1177.

[29] Clark, J.M., Nimlos, M.R., Robichaud, D.J. Comparison of Unimolecular Decomposition Pathways for Carboxylic Acids of Relevance to Biofuels, J. Phys. Chem. A 118 (2014) 260-274.

[30] Mendes, J., Zho, C.-W., Curran, H.J. Theoretical Chemical Kinetic Study of the H-Atom Abstraction Reactions from Aldehydes and Acids by Ḣ Atoms and ȮH, HȮ$_2$, and ĊH$_3$ Radicals, J. Phys. Chem. A 118 (2014) 12089-12104.

[31] Grana, R, Frassoldati, A, Faravelli, T, Niemann, U, Ranzi, E, Seiser, R, Cattolica, R, Seshadri, K. An Experimental and Kinetic Modeling Study of Combustion of Isomers of Butanol, Combust. Flame 15 (2010) 2137-2154.

[32] Sun, W., Tao, T., Zhang, R., Liao, H., Huang, C., Zhang, F., Zhang, X., Zhang, Y., Yang, B. Experimental and Modeling Efforts towards a Better Understanding of the High-Temperature Combustion kinetics of C3-C5 ethyl esters, Combust. Flame 185 (2017) 173-187.

[33] Sivaramakrishnan, R., Michael, J.V. Rate Constants for OH with Selected Large Alkanes: Shock-Tube Measurements and an Improved Group Scheme, J. Phys. Chem. A 113 (2009) 5047-5060.

[34] Dean, A.M., Bozzelli, J.W. Combustion chemistry of nitrogen, in: W.C. Gardiner Jr. (Ed.), Gas-Phase Combustion Chemistry, Springer, New York, 2000, pp. 125–341.

[35] Dayma, G., Halter, F., Foucher, F., Togbé, C., Mounaim-Rouselle, C., Dagaut, P. Experimental and Detailed Kinetic Modeling Study of Ethyl Pentanoate (Ethyl Valerate) Oxidation in a Jet Stirred Reactor and Laminar Burning Velocities in a Spherical Combustion Chamber, Energy Fuels 26 (2012) 435-438.

[36] Sirjean, B., Glaude, P.A., Ruiz-Lopèz, M.F., Fournet, R. Theoretical Kinetic Study of Thermal Unimolecular Decomposition of Cyclic Alkyl Radicals, J. Phys. Chem. A, 112 (2008) 11598-11610.

[37] Allara, D.L., Shaw, R. A Compilation of Kinetic Parameters for the Thermal-Degradation of Normal-Alkane Molecules, J. Phys. Chem. Ref. Data 9 (1980) 523–559.

[38] Larson, C.W., Stewart, P.H., Golden, D.M. Pressure and temperature dependence of reactions proceeding via a bound complex. An approach for combustion and atmospheric chemistry modelers. Application to HO + CO → [HOCO] → H + $CO_2$, Int. J. Chem. Kinet. 20 (1988) 27-40.

[39] Cavallotti, C., Pelucchi, M., Frassoldati, A. Analysis of Acetic Acid Gas phase Reactivity: Rate Constant Estimation and Kinetic Simulations, Proc. Combust. Inst. 3 (2019) 539-546.

[40] Umemoto, H., Tsunashima, S., Sato, S., Washida, N., Hatakeyama, S. The Reactions of Hydrogen and Deuterium Atoms with 4 Ketenes, Bull. Chem. Soc. Jpn. 57 (1984) 2578-2580.

[41] Touchard S., Buda F., Dayma G., Glaude P.A., Fournet R., Battin-Leclerc F. Experimental and Modelling Study of the Oxidation of 1-Pentene at High Temperature, Int. J. Chem. Kinet. 37 (2005) 451-463.

[42] Sumathi, R., Green, W.H. Jr. Thermodynamic Properties of Ketenes: Group Additivity Values from Quantum Chemical Calculations, J. Phys. Chem. A 106 (2002) 7937-7949.

[43] Marshall, P., Glarborg, P. Ab initio and kinetic modeling studies of formic acid oxidation, Proc. Combust. Inst. 35 (2015) 153–160.

[44] Leplat, N., Vandooren, J. Numerical and Experimental Study of the Combustion of Acetic Acid in Laminar Premixed Flames, Combust. Flame 159 (2012) 493-499.

[45] Gasnot, L, Decottignies, V, Pauwels, J.F. Kinetics Modelling of Ethyl Acetate Oxidation in Flame Conditions, Fuel 84 (2005) 505–518.

[46] Lizardo-Huerta, J.-C., Sirjean, B., Verdier, L., Fournet, R., Glaude, P.-A. Kinetic Modeling of the Thermal Destruction of Nitrogen Mustard Gas, J. Phys. Chem.A, 121 (2017) 3254-3262.

[47] Namysl, S., Pelucchi, M., Herbinet, O., Frassoldati, A., Faravelli, T., Battin-Leclerc, F. A first evaluation of butanoic and pentanoic acid oxidation kinetics, Chemical Engineering Journal (2019), doi: https:// doi.org/10.1016/j.cej.2019.05.090.

[48] Gou, Q., Feng, G., Evandelisti, L., Caminati, W. Conformers of Dimers of Carboxylic Acids in the Gas-Phase: A Rotational Study of Difluoroacetic Acid-Formic Acid, Chem. Phys. Lett. 591 (2014) 301-305.

[49] Clark, J.M., Nimlos, M.R., Robichaud, D.J. Bimolecular Decomposition Pathways for Carboxylic Acids of Relevance to Biofuels, J. Phys. Chem. A 119 (2015) 501-516.

## SUPPLEMENTARY MATERIAL

### Appendix A – Equipment used to conduct the experimental study of octanoic acid pyrolysis and analysis of the products formed.

**Figure A1** displays the bench-scale experimental setup that was designed in a previous work [25] and used in this study to carry out octanoic acid pyrolysis under various operating conditions to validate the proposed detailed kinetic model. As shown is **Figure A1**, the reaction product analysis unit comprises prior the $CO/CO_2$ non-dispersive infrared (NDIR) analyzer (Cosma Cristal 300), a gas sampling bulb from which reaction products were withdrawn together with those trapped in upstream U-tubes for analysis by gas chromatography (GC). Details of GC equipment and operating conditions are given in **Table A1**.

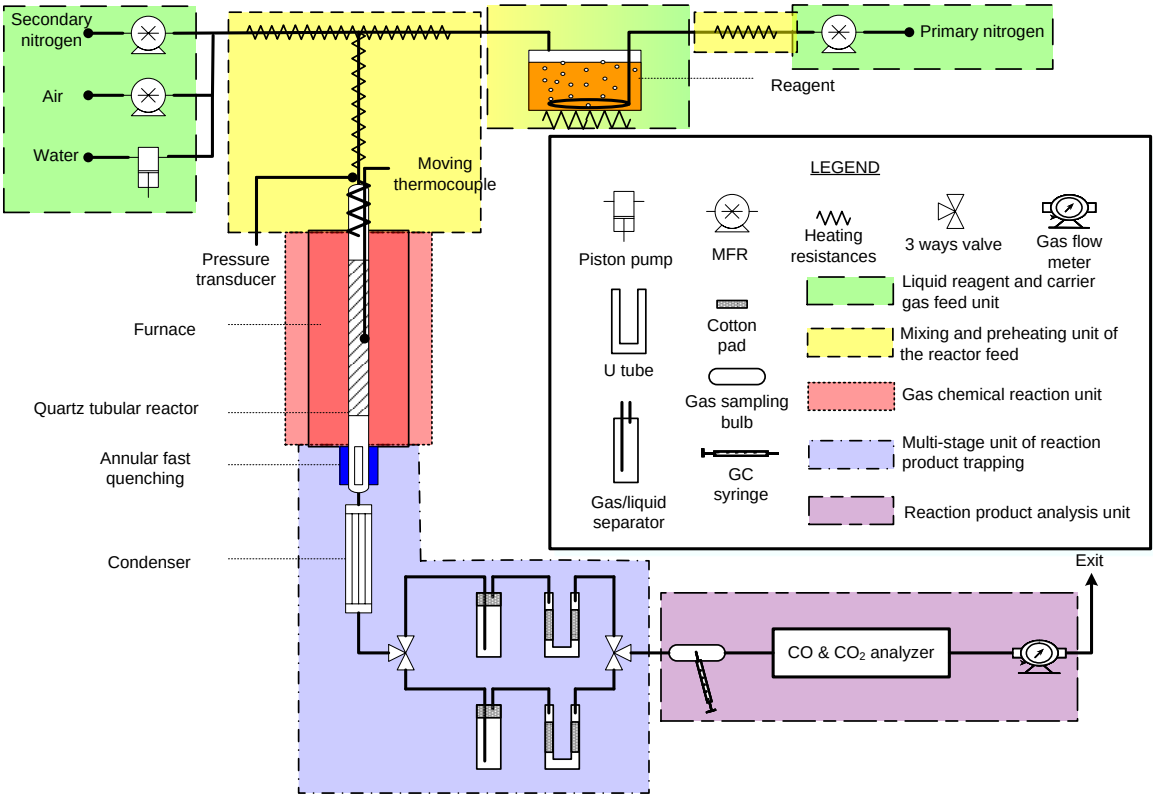


**Figure A1.** Schematic layout of the bench-scale experimental setup [25].[a]

[a] Water supply was planned for possible extension of the experimental setup to steam cracking or steam reforming. The gas-liquid mixture leaving the condenser is sent either to the transient state or to the steady state transfer line, both of them linked together at their extremity by two 3-way valves.

**Table A1.** GC analyses of the octanoic acid pyrolysis products (excluding CO, $CO_2$ and burned off coke analyzed by NDIR).

| Conditions | $H_2$ | Non-condensable gas (excluding $H_2$, CO, and $CO_2$) | Condensate [a] (excluding octanoic acid) | Condensate [a] (exclusively octanoic acid) |
|---|---|---|---|---|
| GC-type | Intersmat IGC 11-type | Schimadzu GC 17A | Schimadzu GC 17A | Stang ST 200 |
| Detector | TCD | FID | FID | FID |
| Detector temperature /°C | - | 310 | 310 | 280 |
| Injector temperature /°C | - | 300 | 300 | 270 |
| Carrier gas ($N_2$) volumetric flow rate (NmL/min) or linear velocity (cm/s) | 30 NmL/min | 15 cm/s | 15 cm/s | 0.91 NmL/min |
| Split ratio | - | 1/100 | 1/100 | 1/160 |
| Column | Silica-gel filled column / molecular sieve (5Å thickness) 5 m length, 6 mm inner diameter | Bonded non-polar (methyl silicone) capillary column (P.O.N.A.-type, Hewlet Packard) 50 m, 0.21 mm, 0.5 μm film thickness | Bonded non-polar (methyl silicone) capillary column (P.O.N.A.-type, Hewlet Packard) 50 m, 0.21 mm, 0.5 μm film thickness | Polyethyleneglycol capillary column (CP-Wax 52CB, Chrompack) 50 m, 0.32 mm, 0.2 μm film thickness |
| Oven temperature program | 60°C | 60°C (4 min), 60-180°C (10°C/min, 10 min), 180-300°C (10°C/min) | 60°C (20 min), 60-300°C (2°C/min, 40 min | 60°C (10 min), 60-240°C (10°C/min, 32 min) |
| Column pressure program | - | 96 kPa (4 min), 96-153 kPa (2.4 kPa/min, 10 min), 153-182 kPa (2.4 kPa/min) | 124 kPa (20 min), 124-182 kPa (0.5 kPa/min, 44 min) | - |

[a] The GC-FID system was calibrated by calculating a carbon response factor compared with the internal standard (IS) both for each identified product and for the unconverted reagent (octanoic acid). To cover a wider range of retention times, two IS were used. As previous tests showed that neither n-octane nor n-dodecane were formed during octanoic acid pyrolysis (under the investigated reaction conditions), n-octane was selected as IS for all observed products whereas n-dodecane was used as IS to quantify the non-converted octanoic acid fraction.

## Appendix B – Experimental results obtained in this work during octanoic acid pyrolysis in PFR

This section displays the experimental data of octanoic acid pyrolysis generated in this work under various operating conditions. **Table B1** gathers the temperature profiles measured along the tubular reactor for the selected oven set point temperatures. **Tables B2-B4** give for each run the selected operating conditions, together with the corresponding material balances and pyrolysis product mole fractions. For each run, the residence time was determined by considering the reactor pressure and the reactor mean temperature (average of the reactor temperature profile values recorded for a given oven set point). **Table B5** [25] concerns experiment repeatability.

**Table B1.** Experimental temperature profiles along the tubular reactor recorded for the oven set point temperatures selected in this work.

| Axial coordinate | Oven set point temperature (K) | | | | |
|---|---|---|---|---|---|
| (z/cm) | 923.15 | 948.15 | 973.15 | 1023.15 | 1073.15 |
| 0 | 590.15 | 597.15 | 581.15 | 593.15 | 599.15 |
| 1 | 590.15 | 597.15 | 581.15 | 593.15 | 599.15 |
| 2 | 590.15 | 602.15 | 581.65 | 597.15 | 610.15 |
| 3 | 590.15 | 607.15 | 582.15 | 601.15 | 621.15 |
| 4 | 604.15 | 632.65 | 601.15 | 630.15 | 655.65 |
| 5 | 618.15 | 658.15 | 620.15 | 659.15 | 690.15 |
| 6 | 647.15 | 697.15 | 657.65 | 703.65 | 725.15 |
| 7 | 676.15 | 736.15 | 695.15 | 748.15 | 760.15 |
| 8 | 712.15 | 771.65 | 747.15 | 795.65 | 804.65 |
| 9 | 748.15 | 807.15 | 789.15 | 843.15 | 849.15 |
| 10 | 783.15 | 838.65 | 825.65 | 883.65 | 890.65 |
| 11 | 818.15 | 870.15 | 862.15 | 924.15 | 932.15 |
| 12 | 847.15 | 896.15 | 891.65 | 953.15 | 958.65 |
| 13 | 876.15 | 922.15 | 921.15 | 982.15 | 985.15 |
| 14 | 896.15 | 936.65 | 945.15 | 998.65 | 1016.65 |
| 15 | 916.15 | 951.15 | 969.15 | 1015.15 | 1048.15 |
| 16 | 923.15 | 955.65 | 976.15 | 1021.15 | 1061.15 |
| 17 | 930.15 | 960.15 | 983.15 | 1027.15 | 1074.15 |
| 18 | 934.15 | 962.65 | 985.15 | 1031.15 | 1078.15 |
| 19 | 939.15 | 965.15 | 987.15 | 1035.15 | 1082.15 |
| 20 | 940.65 | 966.15 | 989.15 | 1035.65 | 1084.15 |
| 21 | 942.15 | 967.15 | 991.15 | 1036.15 | 1086.15 |
| 22 | 942.65 | 967.65 | 991.65 | 1036.65 | 1087.15 |
| 23 | 943.15 | 968.15 | 992.15 | 1037.15 | 1088.15 |
| 24 | 943.65 | 967.65 | 992.15 | 1037.15 | 1088.65 |

**Table B1.** Continued.

| Axial coordinate | Oven set point temperature (K) | | | | |
|---|---|---|---|---|---|
| (z/cm) | 923.15 | 948.15 | 973.15 | 1023.15 | 1073.15 |
| 25 | 944.15 | 967.15 | 992.15 | 1037.15 | 1089.15 |
| 26 | 943.65 | 966.15 | 991.15 | 1037.15 | 1089.15 |
| 27 | 943.15 | 965.65 | 990.15 | 1037.15 | 1089.15 |
| 28 | 942.15 | 963.65 | 989.65 | 1036.15 | 1088.65 |
| 29 | 941.15 | 962.15 | 989.15 | 1035.15 | 1088.15 |
| 30 | 939.65 | 960.65 | 987.65 | 1034.65 | 1085.65 |
| 31 | 938.15 | 959.15 | 986.15 | 1033.15 | 1083.15 |
| 32 | 936.65 | 956.15 | 984.65 | 1031.65 | 1081.65 |
| 33 | 935.15 | 953.15 | 983.15 | 1030.15 | 1080.15 |
| 34 | 932.65 | 950.15 | 981.15 | 1028.65 | 1078.15 |
| 35 | 930.15 | 947.15 | 979.15 | 1027.15 | 1076.15 |
| 36 | 927.15 | 943.65 | 977.15 | 1024.65 | 1072.65 |
| 37 | 924.15 | 940.15 | 975.15 | 1022.15 | 1069.15 |
| 38 | 919.65 | 933.65 | 971.65 | 1019.65 | 1062.65 |
| 39 | 915.15 | 927.15 | 968.15 | 1017.15 | 1056.15 |
| 40 | 909.65 | 918.65 | 963.65 | 1011.65 | 1049.65 |
| 41 | 904.15 | 910.15 | 959.15 | 1006.15 | 1043.15 |
| 42 | 894.15 | 904.15 | 950.65 | 995.65 | 1036.15 |
| 43 | 884.15 | 898.15 | 942.15 | 985.15 | 1029.15 |
| 44 | 881.65 | 886.65 | 935.65 | 984.15 | 1022.15 |
| 45 | 879.15 | 875.15 | 928.15 | 983.15 | 1015.15 |
| 46 | 872.15 | 861.65 | 917.15 | 972.65 | 993.15 |
| 47 | 865.15 | 848.15 | 906.15 | 962.15 | 971.15 |
| 48 | 842.15 | 820.15 | 880.65 | 936.65 | 931.15 |
| 49 | 819.15 | 792.15 | 855.15 | 911.15 | 891.15 |
| 50 | 789.15 | 756.65 | 816.65 | 884.15 | 847.15 |
| 51 | 759.15 | 721.15 | 778.15 | 857.15 | 803.15 |
| 52 | 730.15 | 687.15 | 754.15 | 818.15 | 758.65 |
| 53 | 701.15 | 653.15 | 730.15 | 779.15 | 714.15 |
| 54 | 639.65 | 607.15 | 675.65 | 707.65 | 669.65 |
| 55 | 578.15 | 561.15 | 621.15 | 636.15 | 625.15 |
| Average value (K) | 837.57 | 853.55 | 876.78 | 923.24 | 947.60 |

**Table B2.** Experimental results related to octanoic acid pyrolysis conducted in PFR from 923.15 to 948.15 K.

| Experiment | 1 | 2 | 3 | 4 | 5 | 6 |
|---|---|---|---|---|---|---|
| Oven set point temperature (K) | 923.15 | 923.15 | 923.15 | 948.15 | 948.15 | 948.15 |
| Residence time τ (ms) | 429 | 621 | 843 | 400 | 584 | 796 |
| Pressure (kPa) | 117.7 | 114.9 | 111.6 | 110.4 | 107.2 | 113.7 |
| Octanoic acid mole fraction | 0.046 | 0.050 | 0.052 | 0.052 | 0.054 | 0.052 |
| Conversion of octanoic acid (%, molar basis) | 2.7 | 4.5 | 6.3 | 5.6 | 9.8 | 14.5 |
| Overall material balance (%, mass basis) | 0.0 | 0.0 | 0.0 | 0.0 | 0.0 | 0.0 |
| Material balance in C atom (%, molar basis) | -0.1 | -0.1 | -0.8 | 0.0 | -0.4 | -1.1 |
| Material balance in H atom (%, molar basis) | -0.1 | 0.1 | -0.8 | 1.0 | 0.0 | -0.7 |
| Material balance in O atom (%, molar basis) | 0.4 | 0.4 | 2.8 | 0.0 | 1.1 | 3.8 |
| Chemical species | Component mole fractions (including $N_2$ inert diluent) | | | | | |
| Methane ($CH_4$) | 3.19E-04 | 5.10E-04 | 1.14E-03 | 7.41E-04 | 1.49E-03 | 2.03E-03 |
| Ethylene ($C_2H_4$) | 1.01E-03 | 1.75E-03 | 4.31E-03 | 3.01E-03 | 5.84E-03 | 8.00E-03 |
| Ethane($C_2H_6$) | 0 | - | 3.99E-04 | 1.19E-04 | 1.78E-04 | 0 |
| Propene ($C_3H_6$) | 3.63E-04 | 6.12E-04 | 1.34E-03 | 9.49E-04 | 1.75E-03 | 2.54E-03 |
| n-Propane ($C_3H_8$) | 0 | 0 | 0 | 0 | 0 | 0 |
| 1-Butene ($C_4H_8$) | 1.49E-04 | 2.26E-04 | 4.71E-04 | 3.07E-04 | 6.57E-04 | 1.02E-03 |
| 1,3-Butadiene ($C_4H_6$) | 0 | 0 | 0 | 0 | 0 | 0 |
| n-Butane ($C_4H_{10}$) | 0 | 0 | 0 | 0 | 0 | 0 |
| 1-Pentene ($C_5H_{10}$) | 8.94E-05 | 2.65E-04 | 3.00E-04 | 3.21E-04 | 4.33E-04 | 5.83E-04 |
| n-Pentane ($C_5H_{12}$) | 0 | 0 | 0 | 0 | 0 | 0 |
| 1-Hexene ($C_6H_{12}$) | 1.40E-04 | 3.05E-04 | 5.85E-04 | 3.87E-04 | 6.73E-04 | 7.60E-04 |
| n-Hexane ($C_6H_{14}$ | 0 | 0 | 0 | 0 | 0 | 0 |
| 1-Heptene ($C_7H_{14}$) | 0 | 9.44E-06 | 1.75E-04 | 0 | 0 | 2.43E-04 |
| n-Heptane ($C_7H_{16}$) | 0 | 0 | 0 | 0 | 0 | 0 |
| Acetic acid ($CH_3COOH$) | 1.44E-04 | 7.03E-04 | 2.86E-04 | 2.87E-04 | 8.71E-04 | 5.17E-04 |
| 2-Propenoic acid ($C_2H_3COOH$) | 2.33E-04 | 3.55E-04 | 5.13E-04 | 8.51E-04 | 2.06E-03 | 2.23E-03 |
| Propanoic acid ($C_2H_5COOH$) | 0 | 0 | 0 | 0 | 0 | 0 |
| 3-Butenoic acid ($C_3H_5COOH$) | 0 | 0 | 0 | 0 | 0 | 0 |
| Butanoic acid ($C_3H_7COOH$) | 0 | 0 | 0 | 0 | 0 | 0 |
| 4-Pentenoic acid ($C_4H_7COOH$) | 4.81E-05 | 6.21E-05 | 6.85E-05 | 1.29E-04 | 2.22E-04 | 5.60E-04 |
| Pentanoic acid ($C_4H_9COOH$) | 4.12E-05 | 5.24E-05 | 1.12E-04 | 3.43E-05 | 9.68E-05 | 0 |
| 5-Hexenoic acid ($C_5H_9COOH$) | 1.01E-04 | 1.30E-04 | 1.30E-04 | 2.46E-04 | 3.69E-04 | 8.77E-04 |
| Hexanoic acid ($C_5H_{11}COOH$) | 1.53E-04 | 1.77E-04 | 1.41E-04 | 1.60E-04 | 1.99E-04 | 3.06E-04 |
| 6-Heptenoic acid ($C_6H_{11}COOH$) | 3.84E-05 | 5.22E-05 | 5.25E-05 | 8.70E-05 | 1.02E-04 | 4.11E-04 |
| Heptanoic acid ($C_6H_{13}COOH$) | 3.27E-05 | 3.69E-05 | 3.21E-05 | 3.74E-05 | 3.67E-05 | 1.62E-04 |
| 7-Octenoic acid ($C_7H_{13}COOH$) | 0 | 0 | 0 | 0 | 0 | 0 |
| Octanoic acid ($C_7H_{15}COOH$) | 4.46E-02 | 4.71E-02 | 4.87E-02 | 4.91E-02 | 4.82E-02 | 4.36E-02 |
| Hydrogen ($H_2$) | 1.71E-04 | 2.96E-04 | 4.10E-04 | 4.35E-04 | 7.34E-04 | 8.57E-04 |
| Carbon monoxide (CO) | 0 | 0 | 0 | 0 | 0 | 0 |
| Carbon dioxide ($CO_2$) | 1.76E-04 | 3.71E-04 | 4.52E-04 | 5.38E-04 | 6.25E-04 | 2.76E-04 |
| Coke | 2.01E-04 | 8.19E-04 | 2.24E-04 | 7.04E-04 | 2.12E-04 | 4.68E-04 |
| Nitrogen ($N_2$) | 9.52E-01 | 9.46E-01 | 9.40E-01 | 9.42E-01 | 9.35E-01 | 9.35E-01 |
| Total | 1 | 1 | 1 | 1 | 1 | 1 |

**Table B3.** Experimental results related to octanoic acid pyrolysis conducted in PFR from 973.15 to 1023.15 K.

| Experiment | 7 | 8 | 9 | 10 | 11 | 12 | 13 |
|---|---|---|---|---|---|---|---|
| Oven set point temperature (K) | 973.15 | 973.15 | 973.15 | 973.15 | 1023.15 | 1023.15 | 1023.15 |
| Residence time τ (ms) | 422 | 423 | 655 | 838 | 434 | 623 | 841 |
| Pressure (kPa) | 114.7 | 115.0 | 115.7 | 109.2 | 114.9 | 113.6 | 109.7 |
| Octanoic acid mole fraction | 0.047 | 0.052 | 0.048 | 0.051 | 0.048 | 0.049 | 0.051 |
| Conversion of octanoic acid (%, molar basis) | 7.8 | 9.2 | 16.0 | 21.0 | 19.6 | 28.5 | 36.9 |
| Overall material balance (%, mass basis) | 0.0 | 0.0 | 0.0 | 0.0 | 0.0 | 0.0 | 0.0 |
| Material balance in C atom (%, molar basis) | -0.4 | -0.5 | 0.5 | -1.8 | -1.5 | -0.6 | -4.3 |
| Material balance in H atom (%, molar basis) | -0.3 | -0.3 | 1.7 | -1.0 | -1.1 | 0.6 | -4.5 |
| Material balance in O atom (%, molar basis) | 1.4 | 1.7 | -2.4 | 6.0 | 5.2 | 1.7 | 15.1 |
| Chemical species | Component mole fractions (including $N_2$ inert diluent) | | | | | | |
| Methane ($CH_4$) | 1.17E-03 | 1.35E-03 | 1.39E-03 | 4.31E-03 | 3.22E-03 | 4.08E-03 | 8.88E-03 |
| Ethylene ($C_2H_4$) | 3.98E-03 | 4.62E-03 | 5.44E-03 | 1.30E-02 | 1.42E-02 | 1.79E-02 | 3.50E-02 |
| Ethane($C_2H_6$) | 1.11E-04 | 3.43E-04 | - | 6.34E-04 | 5.70E-04 | 6.29E-04 | 1.46E-03 |
| Propene ($C_3H_6$) | 1.37E-03 | 1.37E-03 | 1.90E-03 | 4.57E-03 | 4.06E-03 | 5.49E-03 | 9.19E-03 |
| n-Propane ($C_3H_8$) | 0 | 0 | 0 | 0 | 0 | 0 | 1.51E-04 |
| 1-Butene ($C_4H_8$) | 4.53E-04 | 4.89E-04 | 6.26E-04 | 1.66E-03 | 1.51E-03 | 2.90E-03 | 2.97E-03 |
| 1,3-Butadiene ($C_4H_6$) | 0 | 0 | 0 | 7.64E-04 | 5.25E-04 | 0 | 1.69E-03 |
| n-Butane ($C_4H_{10}$) | 0 | 0 | 0 | 0 | 0 | 0 | 0 |
| 1-Pentene ($C_5H_{10}$) | 2.97E-04 | 2.97E-04 | 3.01E-04 | 6.83E-04 | 3.04E-04 | 2.60E-04 | 2.59E-04 |
| n-Pentane ($C_5H_{12}$) | 0 | 0 | 0 | 0 | 0 | 0 | 0 |
| 1-Hexene ($C_6H_{12}$) | 4.24E-04 | 4.39E-04 | 5.80E-04 | 9.65E-04 | 6.06E-04 | 2.70E-04 | 2.73E-04 |
| n-Hexane ($C_6H_{14}$ | 0 | 0 | 0 | 0 | 0 | 0 | 0 |
| 1-Heptene ($C_7H_{14}$) | 1.49E-04 | 1.38E-04 | 6.76E-05 | 2.78E-04 | 9.31E-05 | 7.87E-05 | 0 |
| n-Heptane ($C_7H_{16}$) | 0 | 0 | 0 | 0 | 0 | 0 | 0 |
| Acetic acid ($CH_3COOH$) | 4.06E-04 | 4.47E-04 | 1.16E-03 | 1.03E-03 | 8.09E-04 | 1.57E-03 | 1.24E-03 |
| 2-Propenoic acid ($C_2H_3COOH$) | 1.06E-03 | 1.31E-03 | 3.54E-03 | 3.20E-03 | 3.10E-03 | 6.15E-03 | 4.66E-03 |
| Propanoic acid ($C_2H_5COOH$) | 0 | 0 | 0 | 0 | 0 | 0 | 0 |
| 3-Butenoic acid ($C_3H_5COOH$) | 0 | 0 | 0 | 0 | 0 | 0 | 0 |
| Butanoic acid ($C_3H_7COOH$) | 0 | 0 | 0 | 0 | 0 | 0 | 0 |
| 4-Pentenoic acid ($C_4H_7COOH$) | 2.27E-04 | 2.47E-04 | 6.01E-04 | 4.98E-04 | 4.69E-04 | 8.24E-04 | 4.23E-04 |
| Pentanoic acid ($C_4H_9COOH$) | 5.21E-05 | 0 | 2.80E-04 | 0 | 0 | 0 | 0 |
| 5-Hexenoic acid ($C_5H_9COOH$) | 3.00E-04 | 3.30E-04 | 6.66E-04 | 3.93E-04 | 3.13E-04 | 4.90E-04 | 2.56E-04 |
| Hexanoic acid ($C_5H_{11}COOH$) | 1.30E-04 | 3.57E-04 | 5.64E-04 | 2.52E-04 | 1.22E-04 | 1.98E-04 | 1.09E-04 |
| 6-Heptenoic acid ($C_6H_{11}COOH$) | 1.25E-04 | 1.34E-04 | 3.39E-04 | 2.03E-04 | 1.84E-04 | 2.88E-04 | 1.54E-04 |
| Heptanoic acid ($C_6H_{13}COOH$) | 3.35E-05 | 4.05E-05 | 7.96E-05 | 3.65E-05 | 3.06E-05 | 5.60E-05 | 0 |
| 7-Octenoic acid ($C_7H_{13}COOH$) | 0 | 0 | 0 | 0 | 0 | 0 | 0 |
| Octanoic acid ($C_7H_{15}COOH$) | 4.33E-02 | 4.22E-02 | 3.96E-02 | 3.93E-02 | 3.76E-02 | 3.39E-02 | 3.05E-02 |
| Hydrogen ($H_2$) | 7.85E-04 | 9.44E-04 | 1.36E-03 | 1.46E-03 | 2.24E-03 | 3.23E-03 | 3.80E-03 |
| Carbon monoxide (CO) | 2.91E-04 | 0 | 2.46E-04 | 5.01E-04 | 3.74E-04 | 8.57E-04 | 1.18E-03 |
| Carbon dioxide ($CO_2$) | 4.65E-04 | 5.79E-04 | 1.18E-03 | 1.50E-03 | 1.50E-03 | 2.58E-03 | 2.96E-03 |
| Coke | 2.92E-05 | 3.60E-04 | 9.22E-04 | 1.29E-03 | 6.71E-05 | 3.67E-04 | 1.19E-04 |
| Nitrogen ($N_2$) | 9.45E-01 | 9.44E-01 | 9.39E-01 | 9.23E-01 | 9.28E-01 | 9.18E-01 | 8.95E-01 |
| Total | 1 | 1 | 1 | 1 | 1 | 1 | 1 |

**Table B4.** Experimental results related to octanoic acid pyrolysis conducted in PFR at 1073.15 K (experiments 14-16) or for higher dilutions of octanoic acid (experiments 17-19)

| Experiment | 14 | 15 | 16 | 17 | 18 | 19 |
|---|---|---|---|---|---|---|
| Oven set point temperature (K) | 1073.15 | 1073.15 | 1073.15 | 948.15 | 973.15 | 1023.15 |
| Residence time τ (ms) | 422 | 596 | 814 | 430 | 421 | 416 |
| Pressure (kPa) | 113.6 | 105.3 | 104.0 | 109.6 | 106.5 | 106.0 |
| Octanoic acid mole fraction | 0.048 | 0.053 | 0.054 | 0.026 | 0.027 | 0.026 |
| Conversion of octanoic acid (%, molar basis) | 30.6 | 36.5 | 44.9 | 7.6 | 9.4 | 20.1 |
| Overall material balance (%, mass basis) | 0.0 | 0.0 | 0.0 | 0.0 | 0.0 | 0.0 |
| Material balance in C atom (%, molar basis) | -0.4 | -1.9 | -5.0 | -0.5 | -0.5 | -1.7 |
| Material balance in H atom (%, molar basis) | 0.9 | -1.8 | -6.3 | 2.6 | 0.1 | -1.7 |
| Material balance in O atom (%, molar basis) | 2.5 | 6.6 | 18.2 | 0.0 | 1.4 | 6.0 |
| Chemical species | Component mole fractions (including $N_2$ inert diluent) | | | | | |
| Methane ($CH_4$) | 5.25E-03 | 8.82E-03 | 1.36E-02 | 6.43E-04 | 6.75E-04 | 2.13E-03 |
| Ethylene ($C_2H_4$) | 2.44E-02 | 3.70E-02 | 5.34E-02 | 2.55E-03 | 2.84E-03 | 9.11E-03 |
| Ethane($C_2H_6$) | 1.32E-03 | 1.95E-03 | 3.08E-03 | 0 | 0 | 0 |
| Propene ($C_3H_6$) | 5.35E-03 | 7.17E-03 | 9.33E-03 | 7.09E-04 | 8.59E-04 | 2.54E-03 |
| n-Propane ($C_3H_8$) | 0 | 0 | 0 | 0 | 0 | 0 |
| 1-Butene ($C_4H_8$) | 1.57E-03 | 2.09E-03 | 3.03E-03 | 3.25E-04 | 3.76E-04 | 1.10E-03 |
| 1,3-Butadiene ($C_4H_6$) | 1.32E-03 | 1.54E-03 | 1.34E-03 | 0 | 0 | 0 |
| n-Butane ($C_4H_{10}$) | 0 | 0 | 0 | 0 | 0 | 0 |
| 1-Pentene ($C_5H_{10}$) | 0 | 0 | 0 | 1.88E-04 | 1.81E-04 | 2.38E-04 |
| n-Pentane ($C_5H_{12}$) | 0 | 0 | 0 | 0 | 0 | 0 |
| 1-Hexene ($C_6H_{12}$) | 0 | 0 | 0 | 3.13E-04 | 3.21E-04 | 2.88E-04 |
| n-Hexane ($C_6H_{14}$ | 0 | 0 | 0 | 0 | 0 | 0 |
| 1-Heptene ($C_7H_{14}$) | 0 | 0 | 0 | 7.06E-05 | 6.13E-05 | 0 |
| n-Heptane ($C_7H_{16}$) | 0 | 0 | 0 | 0 | 0 | 0 |
| Acetic acid ($CH_3COOH$) | 9.76E-04 | 2.19E-03 | 7.88E-04 | 1.36E-04 | 1.62E-04 | 2.56E-04 |
| 2-Propenoic acid ($C_2H_3COOH$) | 4.71E-03 | 3.82E-03 | 2.40E-03 | 4.32E-04 | 8.57E-04 | 1.26E-03 |
| Propanoic acid ($C_2H_5COOH$) | 0 | 0 | 4.78E-04 | 0 | 0 | 0 |
| 3-Butenoic acid ($C_3H_5COOH$) | 0 | 0 | 0 | 0 | 0 | 0 |
| Butanoic acid ($C_3H_7COOH$) | 0 | 0 | 0 | 0 | 0 | 0 |
| 4-Pentenoic acid ($C_4H_7COOH$) | 3.97E-04 | 3.16E-04 | 1.19E-04 | 9.05E-05 | 1.43E-04 | 1.58E-04 |
| Pentanoic acid ($C_4H_9COOH$) | 0 | 0 | 9.25E-05 | 0 | 3.90E-05 | 1.63E-05 |
| 5-Hexenoic acid ($C_5H_9COOH$) | 2.18E-04 | 1.97E-04 | 1.54E-04 | 1.60E-04 | 2.10E-04 | 1.68E-04 |
| Hexanoic acid ($C_5H_{11}COOH$) | 8.37E-05 | 5.68E-05 | 5.22E-05 | 6.22E-05 | 5.52E-05 | 3.50E-05 |
| 6-Heptenoic acid ($C_6H_{11}COOH$) | 1.50E-04 | 8.24E-05 | 6.25E-05 | 4.24E-05 | 5.79E-05 | 5.98E-05 |
| Heptanoic acid ($C_6H_{13}COOH$) | 1.84E-05 | 0 | 0 | 1.92E-05 | 1.52E-05 | 1.02E-05 |
| 7-Octenoic acid ($C_7H_{13}COOH$) | 0 | 0 | 0 | 0 | 0 | 0 |
| Octanoic acid ($C_7H_{15}COOH$) | 3.19E-02 | 3.15E-02 | 2.71E-02 | 2.40E-02 | 2.42E-02 | 2.05E-02 |
| Hydrogen ($H_2$) | 4.19E-03 | 6.36E-03 | 6.87E-03 | 2.05E-04 | 4.31E-04 | 1.59E-03 |
| Carbon monoxide (CO) | 2.19E-03 | 2.76E-03 | 3.27E-03 | 0 | 0 | 4.75E-04 |
| Carbon dioxide ($CO_2$) | 5.16E-03 | 6.77E-03 | 7.31E-03 | 3.53E-04 | 5.85E-04 | 1.37E-03 |
| Coke | 0 | 2.45E-04 | 5.29E-04 | 4.09E-04 | 4.66E-04 | 3.09E-04 |
| Nitrogen ($N_2$) | 9.11E-01 | 8.87E-01 | 8.67E-01 | 9.69E-01 | 9.67E-01 | 9.58E-01 |
| Total | 1 | 1 | 1 | 1 | 1 | 1 |

**Table B5.** Repeatability of experiments: standard deviations and coefficients of variation [25].[a]

| Experiment | 7 | 8 | Mean | Standard deviation | Coefficient of variation (%) |
|---|---|---|---|---|---|
| Oven set point temperature (K) | 973.15 | 973.15 | 973.15 | 0.0 | 0.0 |
| Reactor pressure (kPa) | 114.7 | 115.0 | 114.9 | 1.4 | 0.2 |
| Residence time τ (ms) | 422 | 423 | 423 | 0.8 | 0.2 |
| Conversion of reactant (%, molar basis) | 7.8 | 9.2 | 8.0 | 0.7 | 8.5 |
| Material balance in C atom (%, molar basis) | -0.4 | -0.5 | -0.4 | 0.1 | 0.2 |
| Material balance in H atom (%, molar basis) | -0.3 | -0.3 | -0.3 | 0.0 | 0.0 |
| Material balance in O atom (%, molar basis) | 1.4 | 1.7 | 1.6 | 0.2 | 12.5 |
| Chemical species | Molar fractions ($N_2$ diluent-free) % | | | | |
| Methane ($CH_4$) | 2.13 | 2.40 | 2.27 | 0.14 | 6.1 |
| Ethylene ($C_2H_4$) | 7.21 | 8.23 | 7.72 | 0.51 | 6.6 |
| Propene ($C_3H_6$) | 2.48 | 2.43 | 2.46 | 0.02 | 1.0 |
| 1-Butene ($C_4H_8$) | 0.82 | 0.87 | 0.85 | 0.03 | 3.0 |
| 1-Pentene ($C_5H_{10}$) | 0.54 | 0.53 | 0.53 | 0.01 | 1.0 |
| 1-Hexene ($C_6H_{12}$) | 0.77 | 0.78 | 0.77 | 0.01 | 0.8 |
| 1-Heptene ($C_7H_{14}$) | 0.27 | 0.25 | 0.26 | 0.01 | 4.9 |
| Acetic acid ($CH_3COOH$) | 0.74 | 0.80 | 0.77 | 0.03 | 3.9 |
| 2-Propenoic acid ($C_2H_3COOH$) | 1.92 | 2.32 | 2.12 | 0.20 | 9.7 |
| 4-Pentenoic acid ($C_4H_7COOH$) | 0.41 | 0.44 | 0.43 | 0.01 | 3.5 |
| 5-Hexenoic acid ($C_5H_9COOH$) | 0.54 | 0.59 | 0.57 | 0.02 | 3.7 |
| 6-Heptenoic acid ($C_6H_{11}COOH$) | 0.23 | 0.24 | 0.23 | 0.01 | 2.7 |
| Octanoic acid ($C_7H_{15}COOH$) | 78.42 | 75.14 | 76.78 | 1.64 | 2.1 |
| Hydrogen ($H_2$) | 1.42 | 1.68 | 1.55 | 0.13 | 8.3 |
| Carbon monoxide (CO) | 0.53 | 0.00 | 0.26 | 0.26 | 100.0 |
| Carbon dioxide ($CO_2$) | 0.84 | 1.03 | 0.94 | 0.09 | 10.0 |

[a] The highest values of the coefficient of variation are obtained for analysis of CO and $CO_2$. This feature results very likely from the analytical method selected for quantifying these components (NDIR analyzer). Indeed, for the two concerned experiments (7-8), the observed levels of CO and $CO_2$ were in the low limits of detection of the equipment (involving thus larger errors of measurements). Regarding the other species, values of the coefficient of variation are inferior to 10%, which is acceptable for GC analyses. As a result, it can be said that experiments for octanoic acid pyrolysis carried out in this work show a satisfactory repeatability.

## Appendix C – Main features of EXGAS version used in this work

The reaction mechanism provided by EXGAS comprises three parts that operate together: *(i)* a periodically updated $C_0$-$C_2$ reaction base involving all the reactions of species with less than three carbon atoms; *(ii)* a comprehensive primary mechanism in which the only molecular reactant is the initial organic compound, i.e. OA here, which can be converted by unimolecular initiations involving C-C bond breaking, isomerizations of radicals through cyclic transition state and H-atom transfer, decompositions of radicals by β-scission with C-C, C-O or C-H bond breaking, H-abstractions between the initial reactant and radicals, and combinations/dismutations of radicals; *(iii)* a secondary mechanism in which the molecular products of the primary mechanism are consumed by non-elementary reactions (i.e. successive decomposition reactions) promoting formation of $C_{2+}$ radicals, the reactions of which are already included in the primary mechanism; moreover, in order to get a secondary mechanism of manageable size, the reactants are here lumped species (i.e. the isomer molecules formed in the primary mechanism are merged into one unique species).

The thermodynamic properties of the molecules and radicals involved in the generated mechanism are determined by THERGAS software **[28]** using Benson group contribution method **[27]**, and are stored as NASA polynomials with 14 coefficients according to the CHEMKIN II formalism **[15]**. The kinetic data of unimolecular decompositions, isomerizations, and combinations are determined by KINGAS software using the thermochemical kinetic methods based on the transition state theory or the modified collision theory **[27]**. The kinetic data that cannot be determined by KINGAS software are estimated either from correlations based on quantitative structure – reactivity relationships **[16,18,23]**.

Nevertheless, some changes had to be made in this work to the whole generated reactional mechanism in order to render the chemical specificity of the carboxylic group. These changes are briefly described in **Table C1**.

**Table C1.** Main changes made in this work to the whole of the generated reactional mechanism In order to take into account the specific chemistry of carboxylic acids. **(a)** Primary mechanism. Please, refer to **Figure 1** for octanoic acid (OA) bond labels.

| Reaction | Kinetic data source | Comments |
|---|---|---|
| *1- Molecular elimination* | | |
| 1.1- $C_7H_{15}COOH \rightarrow CO_2 + C_7H_{16}$ | Clark et al. [29] | Decarboxylation with alkane formation |
| 1.2- $C_7H_{15}COOH \rightarrow H_2O + C_6H_{13}$-CH=C=O | Clark et al. [29] | Two sets of rate parameters differentiate the two dehydration pathways leading to ketene formation from carboxylic acids with α-hydrogens: *(i)* concerted process; *(ii)* two-step process via an intermediate 1,1-enediol, the formation of which is the limiting step. |
| *2a- H-atom abstraction by $R^\bullet$ = $^\bullet H$, $^\bullet OH$, $^\bullet CH_3$, $^\bullet C_2H_5$* | | |
| 2a.1- from the carboxylic group (COOH) of OA (i.e. O-$H_{49}$ bond) | Mendes et al. [30] | $R^\bullet \neq {}^\bullet C_2H_5$ |
| | Grana et al. [31] | $R^\bullet = {}^\bullet C_2H_5$; rate constants determined by analogy with Grana et al. work [31] |
| 2a.2- from the $CH_2$ group in α-position of the COOH group (i.e. C-$H_{56}$ bonds) or from the $CH_3$ group ending the acid aliphatic chain (i.e. C-$H_{50}$ bonds) | Sun et al. [32] | $R^\bullet \neq {}^\bullet C_2H_5$; propanoic acid sub-mechanism |
| | Buda et al. [18] | $R^\bullet = {}^\bullet C_2H_5$ |
| 2a.3- from the $CH_2$ groups in the acid aliphatic chain excluding the previous ones (i.e. C-$H_{51}$ with k = 51, 52, 53 54 or 55 bonds) | Sivaramakrishnan and Michael [33] | $R^\bullet = {}^\bullet OH$ |
| | Buda et al. [18] | $R^\bullet \neq {}^\bullet OH$; for a given H-abstractor $R^\bullet$, same rate constants for C-$H_{51}$ to C-$H_{55}$ |
| *2b- H-abstraction by $R_1^\bullet$ = $^\bullet COOH$ or $R_2^\bullet$ = $^\bullet CH_2$-$(CH_2)_k$-COOH with k = 0 to 5* | | |
| 2b.1- from the carboxylic group (COOH) of OA (i.e. O-$H_{49}$ bond) | This work | $^\bullet$COOH radical considered as $^\bullet CH_3$ and $^\bullet CH_2$-$(CH_2)_k$-COOH with $k$ = 0 to 5 considered as $^\bullet C_2H_5$ (rate constants different for $R_1^\bullet$ and $R_2^\bullet$ but identical for all $R_2^\bullet$ radicals) |
| 2b.2- from the $CH_2$ group in α-position of the COOH group (i.e. C-$H_{56}$ bonds) | Dean and Bozzelli [34] | $^\bullet$COOH radical considered as $^\bullet$CHO and $^\bullet CH_2$-$(CH_2)_k$-COOH with $k$ = 0 to 5 considered as $^\bullet C_2H_5$ (rate constants different for $R_1^\bullet$ and $R_2^\bullet$ but identical for all $R_2^\bullet$ radicals) |
| 2b.3- from the $CH_3$ group ending the acid aliphatic chain (i.e. C-$H_{50}$ bonds) | Buda et al. [18] | as above |
| 2b.4- from the $CH_2$ groups in the acid aliphatic chain excluding the previous ones (i.e. C-$H_{51}$ with $k$ = 51, 52, 53 54 or 55 bonds) | Buda et al. [18] | $^\bullet$COOH considered as tertiary radical and $^\bullet CH_2$-$(CH_2)_k$-COOH with $k$ = 0 to 5 considered as primary radicals (rate constants different for $R_1^\bullet$ and $R_2^\bullet$ but identical for all $R_2^\bullet$ radicals) |

**Table C1a.** Continued.

| Reaction | Kinetic data source | Comments |
|---|---|---|
| *3- Unimolecular decompositions (initiations)* | | |
| 3.1- by C-C bond rupture | Dayma et al. [35] | Pressure dependent rate constants; Arrhenius pre-exponential factor of reaction: $C_7H_{15}COOH \rightarrow {}^{\bullet}C_6H_{13} + {}^{\bullet}CH_2\text{-}COOH$ was divided by 5 for a better agreement with the experimental data. |
| 3.2- by rupture of the carboxylic O-H or C-O bond | This work | Rate constants estimated from KINGAS [16] based on modified collision theory by Benson [27] |
| *4- Isomerization of octanoic acid radicals formed by H-abstractions* | Buda et al. [18] | Analogy with isomerization of alkyl radicals |
| *5- Homolytic β-scission of the C-H bond in α or β-position of the COOH group for the C3 to C8 radicals derived from OA to form respectively α,β- or β,γ-unsaturated carboxylic acids* | Sirjean et al. [36] | Evans Polanyi correlation |
| *6- Combinations of* | | |
| 6.1- octanoic acid radicals with ${}^{\bullet}H$ or ${}^{\bullet}CH_3$ | This work | Rate constants estimated from KINGAS [16] based on modified collision theory by Benson [27] |
| 6.2- ${}^{\bullet}CH_2COOH + {}^{\bullet}C_2H_5 \rightarrow C_3H_7COOH$ | This work | Arrhenius pre-exponential factor value from Allara et al. [37] divided by 10 for a better agreement with experiments |

**Table C1.** Main changes made in this work to the whole of the generated reactional mechanism In order to take into account the specific chemistry of carboxylic acids. **(b)** Secondary mechanism.

| Reaction | Kinetic data source | Comments |
|---|---|---|
| *1- Sub-mechanisms of formic (HCOOH)and acetic ($CH_3COOH$) acids by Sun et al. [32]* | Sun et al. [32] | Some changes were made to the work by Sun et al. [32] as mentioned in the following. |
| *2- Changes to HCOOH sub-mechanism by Sun et al. [32]* | | |
| 2.1- H-(C=O)OH + $^{\bullet}CH_3$ = H-(C=O)O$^{\bullet}$ + $CH_4$<br>H-(C=O)OH + $^{\bullet}CH_3$ = $^{\bullet}$(C=O)OH + $CH_4$ | Mendes et al. [30] | Reactions not considered by Sun et al. [32] |
| 2.2- $^{\bullet}$(C=O)OH = $CO_2$ + H$^{\bullet}$<br>$^{\bullet}$(C=O)OH = CO + $^{\bullet}$OH | Larson et al. [38] | Pressure dependency of the rate constants is considered. |
| *3- Changes to $CH_3COOH$ sub-mechanism by Sun et al. [32]* | | |
| 3.1- $^{\bullet}CH_2COOH$ = $CH_2$=C=O + $^{\bullet}$OH and<br>$^{\bullet}CH_2COOH$ = $CH_3COO^{\bullet}$ | This work | Kinetic parameters determined by *ab initio* calculations |
| 3.2- $CH_3COOH \rightarrow CH_2$=C=O + $H_2O$ | Clark et al. [29] | Rate constant of the enediol formation (limiting step of the two-step dehydration process) |
| 3.3- H-abstraction by $^{\bullet}$H, $^{\bullet}$OH, and $^{\bullet}CH_3$ from the carboxylic group (COOH) leading to $CH_3COO^{\bullet}$ | Cavallotti et al. [39] | Rate estimations were performed at a higher level of theory than that used by Sun et al. [32]. |
| *4- Hexyl ketene ($C_6H_{13}$-CH=C=O) consumption via:* | | |
| 4.1- H$^{\bullet}$ addition on C=O or on CH=C bond leading respectively to acrolein and $^{\bullet}C_5H_{11}$ radical or to CO and $^{\bullet}C_7H_{15}$ radical | Umemoto et al. [40] | Same rate constants for both reactions |
| 4.2- H-abstraction by $^{\bullet}$H, $^{\bullet}CH_3$, and $^{\bullet}C_2H_5$ from the hexyl chain followed by lumped decomposition | Buda et al. [18] | Detailed kinetic model for auto-ignition of alkanes from $C_4$ to $C_{10}$ |
| *5- $^{\bullet}$H and $^{\bullet}CH_3$ additions on the $CH_2$=CH- bond of monounsaturated carboxylic acids (ethylenic bond located at the opposite aliphatic chain extremity from the carboxylic group): $CH_2$=CH-$(CH_2)_n$-COOH with n = 0 et 5* | Touchard et al. [41] | H$^{\bullet}$ addition on $CH_2$= leads to $CH_3$-CH$^{\bullet}$-$(CH_2)_n$-COOH and on =CH- to $^{\bullet}CH_2$-$CH_2$-$(CH_2)_n$-COOH<br>Same rate constants as their homologous alkenes |
| *6- Retro-ene decomposition of C6-C8 unsaturated carboxylic acids $CH_2$=CH-$(CH_2)_n$-COOH with n = 3 to 4 yielding $CH_3$-CH=$CH_2$ and $CH_2$=CH-$(CH_2)_{n-3}$-COOH* | Touchard et al. [41] | Decomposition of 7-octenoic acid was set as following:<br> 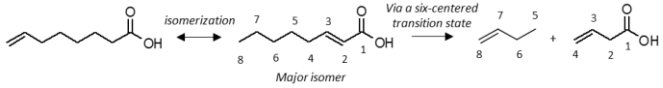 <br><br>Same rate constants as their homologous alkenes |

**Table C1b.** Continued.

| Reaction | Kinetic data source | Comments |
|---|---|---|
| *7- H-abstraction by R• = •H, •OH, •$CH_3$, and •$C_2H_5$ of secondary carboxylic acids (i.e. produced from the primary mechanism, so shorter than the reactant OA)* | | |
| 7.1- from the $CH_2$ group of the acid aliphatic chain | Buda et al. **[18]** | Lumped reactions encompassing H-abstraction and successive decomposition |
| 7.2- from the carboxylic group (COOH) | This work | |

## Appendix D – Overall scheme of octanoic acid decomposition by pyrolysis as proposed in this work

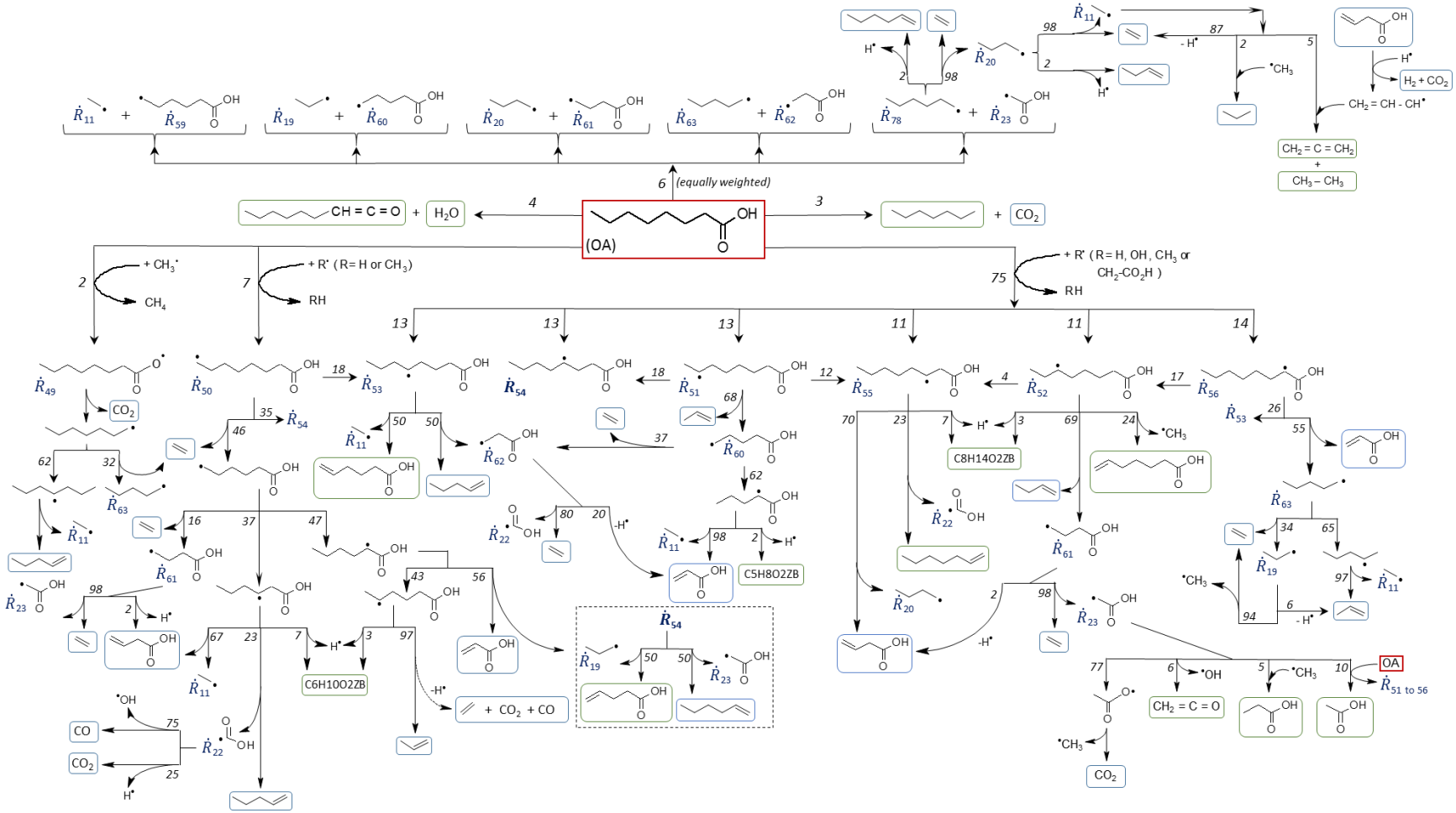


**Figure D1.** Overall scheme of decomposition of octanoic acid (OA) at 1 atm and 1087 K for 421 ms residence time and 5% molar OA in $N_2$ (oven set point temperature: 1073.15 K; PFR axial coordinate: 22 cm; 30% conversion of OA). Italic numbers indicate percent of parent species being converted to daughter species. C5H8O2ZB, C6H10O2ZB and C8H14O2ZB are globalized species taking into account isomers from which the major forms are respectively: $CH_2$=CH-$CH_2$-$CH_2$-COOH, $CH_2$=CH-$(CH_2)_3$-COOH, and $CH_2$=CH-$(CH_2)_3$-COOH.

## Appendix E – Comparison between experiments and modeling for different octanoic acid mole fractions in nitrogen as diluent

This section shows the impact of the reactant dilution on the modelling performance through **Figure E1** which is briefly commented in the main text.

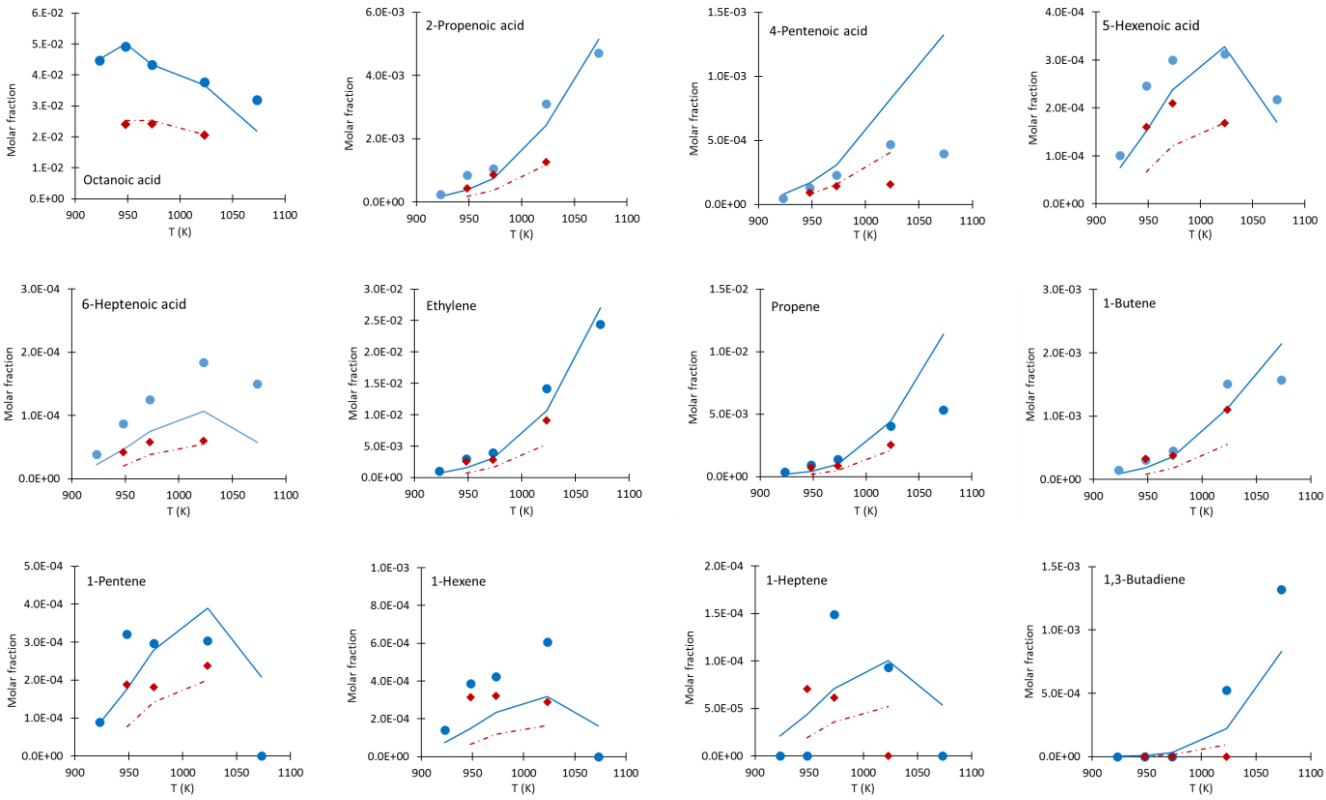


**Figure E1.** Reactant and product mole fraction profiles vs oven set point temperature resulting from octanoic acid pyrolysis carried out in a plug flow reactor at 1 atm for various mole fractions of the reactant in $N_2$: 5.0% for ● and ——; 2.6% for ♦ and -·-·-· (421 ms residence time). Symbols are experimental results and lines are model simulations. ). Butanoic acid, 3-butenoic acid, and 7-octenoic acid were not observed experimentally, and thus were not plotted (as well propanoic acid and propane which were detected only near 1075 K and 826 ms with a mole fraction of 0.05 and 0.02% respectively).

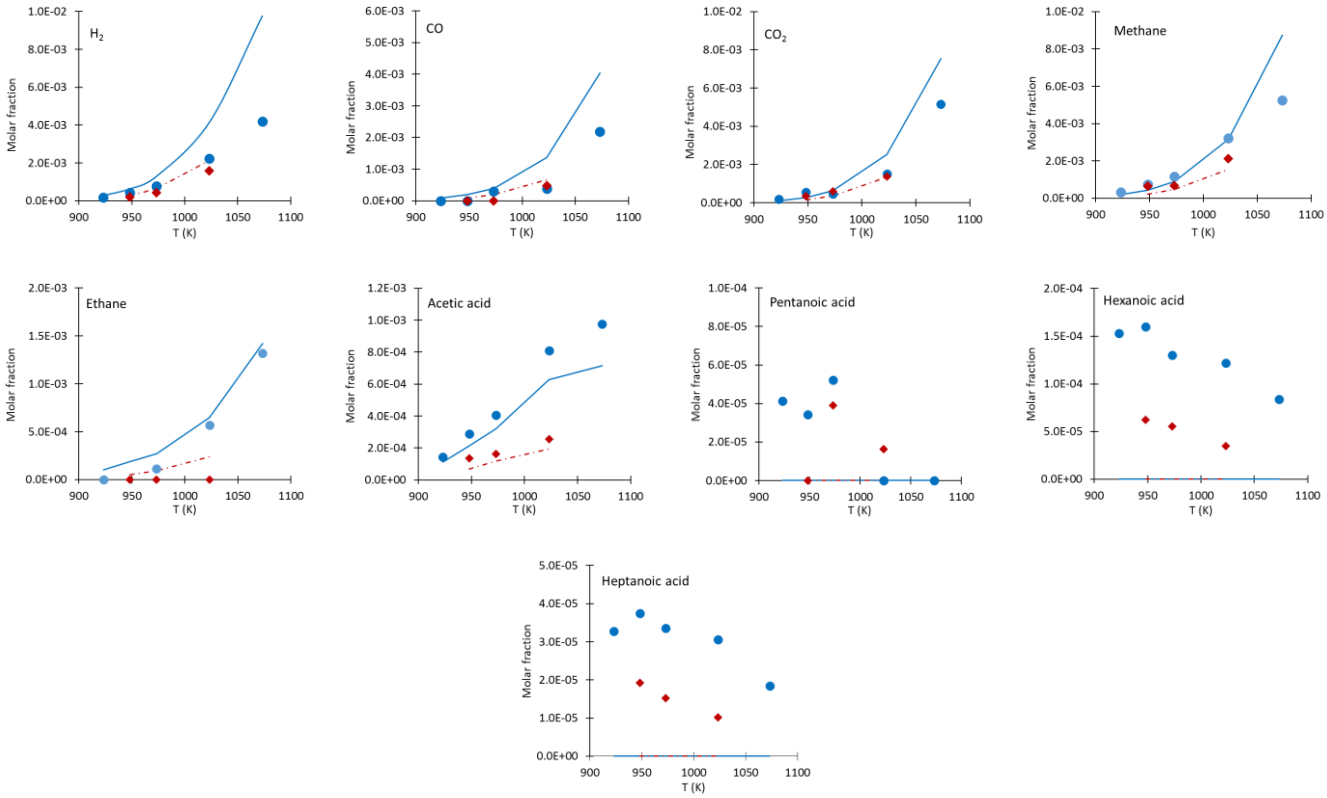


**Figure E1.** Continued.